Development 139, 3531-3542 (2012) doi:10.1242/dev.082222

Myocardin-like protein 2 regulates TGFβ signaling in embryonic stem cells and the developing vasculature

Jian Li[1,2], Nina Bowens[1,3], Lan Cheng[1,2], Xiaohong Zhu[1,2], Mary Chen[1,2], Sridhar Hannenhalli[4], Thomas P. Cappola[1,2] and Michael S. Parmacek[1,2,*]

SUMMARY

The molecular mechanisms that regulate and coordinate signaling between the extracellular matrix (ECM) and cells contributing to the developing vasculature are complex and poorly understood. Myocardin-like protein 2 (MKL2) is a transcriptional co-activator that in response to RhoA and cytoskeletal actin signals physically associates with serum response factor (SRF), activating a subset of SRF-regulated genes. We now report the discovery of a previously undescribed MKL2/TGFβ signaling pathway in embryonic stem (ES) cells that is required for maturation and stabilization of the embryonic vasculature. *Mkl2*$^{-/-}$ null embryos exhibit profound derangements in the tunica media of select arteries and arterial beds, which leads to aneurysmal dilation, dissection and hemorrhage. Remarkably, TGFβ expression, TGFβ signaling and TGFβ-regulated genes encoding ECM are downregulated in *Mkl2*$^{-/-}$ ES cells and the vasculature of *Mkl2*$^{-/-}$ embryos. The gene encoding TGFβ2, the predominant TGFβ isoform expressed in vascular smooth muscle cells and embryonic vasculature, is activated directly via binding of an MKL2/SRF protein complex to a conserved CArG box in the TGFβ2 promoter. Moreover, *Mkl2*$^{-/-}$ ES cells exhibit derangements in cytoskeletal organization, cell adhesion and expression of ECM that are rescued by forced expression of TGFβ2. Taken together, these data demonstrate that MKL2 regulates a conserved TGF-β signaling pathway that is required for angiogenesis and ultimately embryonic survival.

KEY WORDS: Angiogenesis, Embryonic stem cell, Myocardin-related transcription factor B/MKL2, Mouse, Transforming growth factor β

INTRODUCTION

Angiogenesis and vascular patterning are dependent upon the capacity of vascular smooth muscle cells (SMCs) to transduce biomechanical and humoral signals that influence cell differentiation, migration, proliferation and survival (Owens, 1998; Owens et al., 2004). Under homeostatic conditions, vascular SMCs assume a spindle-like morphology with a rich, well-organized cytoskeleton expressing abundant SMC-restricted contractile proteins that together define the contractile properties of this muscle cell lineage. Within the arterial wall, signals transduced directly from endothelial cells and the extracellular matrix (ECM) regulate the physiological properties of SMCs (Astrof and Hynes, 2009; Hayward et al., 1995; Thyberg and Hultgårdh-Nilsson, 1994). The signals transduced between ECM components and vascular SMCs play crucial roles in regulating embryonic angiogenesis and contribute to pathogenesis of atherosclerosis and the formation of arterial aneurysms (Raines, 2000).

Our group and others have shown that the MADS box transcription factor, serum response factor (SRF), acting in concert with transcriptional co-activators in the myocardin-related transcription factor (MRTF) family, including myocardin, myocardin-like protein 1 (MKL1) and myocardin-like protein 2 (MKL2), promote the contractile SMC phenotype (Parmacek, 2007). Forced expression of any member of the MRTF family in embryonic stem (ES) cells activates transcription of endogenous genes encoding SMC-restricted contractile proteins (Du et al., 2004; Du et al., 2003). In response to Rho/actin signaling, MKL1 and MKL2 localize to the nucleus where they physically associate with SRF and activate transcription of a subset of genes associated with cytoskeletal organization (Sotiropoulos et al., 1999).

Two lines of genetically engineered mice that harbor loss-of-function mutations in the *Mkl2* gene have been described (Li et al., 2005; Oh et al., 2005; Wei et al., 2007). Mice containing an *Mkl2* insertional gene trap mutation located between exons 10 and 11 exhibit a hypomorphic phenotype. Gene trap mutant mice survive to birth, but die within 48 hours, exhibiting a spectrum of cardiac outflow tract and great artery patterning defects that are attributable to a cell-autonomous block in differentiation of neural crest-derived vascular SMCs (Li et al., 2005; Wei et al., 2007). Defects in development of the vitelline system that produces the liver sinusoids are also observed in *Mkl2* gene trap mutant embryos (Wei et al., 2007). By contrast, *Mkl2*$^{-/-}$ embryos survive until embryonic day (E) 13.5-14.5 and they also demonstrate defective remodeling of the pharyngeal arch arteries and cardiac outflow tract, recapitulating common forms of congenital heart disease (Oh et al., 2005). In addition, *Mkl2*$^{-/-}$ embryos develop pericardial edema and hemorrhage (Oh et al., 2005). However, the observed defects in vascular patterning in *Mkl2*$^{-/-}$ null embryos fails to explain lethality at mid-gestation, raising questions of what other functions are mediated by MKL2 in differentiating cells and the embryo.

Multiple studies have shown that TGFβ signaling plays a crucial role in development of the great arteries (Pardali et al., 2010). TGFβ signaling influences vascular SMC shape, migration, homing and location through processes that are controlled by cell-surface transmembrane receptors and components of the extracellular matrix (ECM) (Massagué, 1990). TGFβ2 and, to a lesser extent, TGFβ3 are expressed by vascular SMCs (Molin et al., 2003). Genetic studies in mice and humans have shown that

[1]University of Pennsylvania Cardiovascular Institute, University of Pennsylvania, Philadelphia, PA 19104-4283, USA. [2]Department of Medicine, University of Pennsylvania, Philadelphia, PA 19104-4283, USA. [3]Department of Surgery, University of Pennsylvania, Philadelphia, PA 19104-4283, USA. [4]University of Maryland Center for Bioinformatics and Computational Biology, College Park, MD 20742, USA.

*Author for correspondence (michael.parmacek@uphs.upenn.edu)

Accepted 6 July 2012

disruption of TGFβ signaling pathways results in defects in vasculogenesis and angiogenesis that are attributable, at least in part, to vascular SMCs (Pardali et al., 2010). Mice in which the *Tgbr2* gene was conditionally ablated in vascular SMC precursors display arterial dilation and aneurysm formation, which leads to late embryonic lethality (Choudhary et al., 2009).

To examine the function of MKL2 in the developing embryo, we generated and characterized *Mkl2*$^{-/-}$ ES cells and mouse embryos. By mid-gestation, *Mkl2*$^{-/-}$ embryos develop aneurysmal dilation and dissection of the aorta, carotid arteries and select arterial beds throughout the embryo. *Mkl2*$^{-/-}$ mutant arteries display disruption of the tunica media with alterations in SMC morphology, alignment and investment of ECM. Surprisingly, analysis of *Mkl2*$^{-/-}$ ES cells revealed defects in cell adhesion that are attributable to a block in TGFβ signaling and TGFβ-regulated genes that encode ECM. Consistent with these data, TGFβ expression, TGFβ signaling and the expression of TGFβ-regulated genes encoding ECM are disrupted in the vasculature of *Mkl2*$^{-/-}$ embryos. Moreover, *Tgfb2* is activated directly via binding of an MKL2/SRF complex to the *Tgfb2* promoter. These data reveal an MKL2/TGFβ-dependent signaling pathway in ES cells that is also required for development and structural integrity of the embryonic vasculature.

MATERIALS AND METHODS

Generation and characterization of *Mkl2* null mice

An *Mkl2* gene-targeting vector was constructed via recombineering with a BAC (BAC/PAC Resources, clone number BAC RP23-402A16) as described previously (Lee et al., 2001) (supplementary material Fig. S1). Conditionally targeted *Mkl2*$^{+/F}$ ES cells were transiently transfected with the pCMV-Cre expression plasmid to generate heterozygous *Mkl2*$^{+/-}$ ES cells. *Mkl2*$^{+/-}$ ES cells were re-targeted via electroporation with the linearized *Mkl2* conditional targeting vector (supplementary material Fig. S1A). *Mkl2*$^{-/F}$ ES cells were transfected with the pTurbo-Cre plasmid (Washington University, St Louis, MO) generating homozygous *Mkl2*$^{-/-}$ ES cells. To generate *Mkl2*$^{-/-}$ ES cells that stably express TGFβ2, *Mkl2*$^{-/-}$ and wild-type ES cells were stably transfected with the pIRES2-TGFβ2-EGFP vector that expresses TGFβ2 and EGFP. Conditionally targeted *Mkl2*$^{+/F}$ ES cells were microinjected into C57BL/6 donor blastocysts as described previously (Morrisey et al., 1998). Southern blot analysis was performed to confirm that the conditionally targeted *Mkl2*$^{+/F}$ allele was passed through the germline (supplementary material Fig. S1). To create a germline mutation in the *Mkl2* gene, *Mkl2*$^{F/F}$ mice were interbred with *CMV-Cre* transgenic mice. Genotype analyses were performed by Southern blot or by PCR as described previously (Li et al., 2005). PCR genotyping primers can be found in supplementary material Table S1. All animal experimentation was performed under protocols approved by the University of Pennsylvania IACUC and in accordance with NIH guidelines.

Histology and immunohistochemistry

Standard histology and immunohistochemistry protocols are available at http://www.med.upenn.edu/mcrc/histology_core (IHC in paraffin section and H&E staining) and http://www.med.upenn.edu/mcrc/histology_core/culturedcells/shtml. F-actin expression was assessed by staining with rhodamine-tagged phalloidin (Invitrogen, catalog code R415) and G-actin was identified with FITC-stained DNase I (Invitrogen, catalog code D12371). A list of the antibodies used is provided in supplementary material Table S2.

Immunoblot and ELISA analyses

Immunoblot analyses were performed as described previously (Li et al., 2005). The concentration of secreted fibronectin in ES cells was determined using the mouse fibronectin ELISA (Cell Application, catalog code CL0351). ES cells (1.0×10^6/well) were seeded in six-well plates with 2 ml medium for 1 hour and the medium was collected for measurement of secreted fibronectin. Data are expressed as ng fibronectin/ml±s.e.m.

Microarray analysis

Total RNA was extracted from wild-type and *Mkl2*$^{-/-}$ ES cells using the RNeasy protocol (Invitrogen), yielding RNA for two wild-type and three *Mkl2*$^{-/-}$ samples. Each sample was hybridized with Affymetrix Mouse Gene ST 1.0 microarrays according to standard protocols. Raw.cel files were normalized using the RMA algorithm, and exploratory analyses compared fold change in expression in *Mkl2*$^{-/-}$ versus control. These data were deposited in the Gene Expression Omnibus (GEO) public database (Accession Number GSE38316). To screen for signaling pathways affected by *Mkl2* deletion, Gene Set Enrichment Analysis (GSEA) was performed using all signaling pathways described in the Kyoto Encyclopedia of Genes and Genomes (KEGG) in the Molecular Signature Database (Subramanian et al., 2005).

qRT-PCR

The sequences of the PCR primers are listed in supplementary material Table S1. Target genes were amplified by PCR with Power SYBR green (Applied Biosystems, catalog number 4309155) as described previously (Du et al., 2004). All reactions were run in triplicate, and relative gene expression was calculated against a GAPDH standard as described previously (Du et al., 2004). Data are expressed as mean gene expression (arbitrary units)±s.e.m.

Transient transfection analyses

The pTGFβ2.luc luciferase reporter plasmid contains the mouse 1.7 kb mouse TGFβ2 promoter subcloned into pGL3-Basic plasmid (Promega). The pTGFβ2 μCArG1.luc plasmid is identical to pTGFβ2.luc, except the TGFβ2 promoter contains a 2 bp mutation in CArG1 that abolishes binding of SRF to the TGFβ2 promoter. Cos-7 cells (2×10^5/well) were transiently co-transfected with 400 ng luciferase reporter plasmid, 100-400 ng of pcDNA3 control or pcDNA3-based expression plasmid and 5ng *Renilla* reference plasmid (pRL-TK) using Lipofectamine 2000 (Invitrogen). Luciferase and *Renilla* assays were performed with the Dual-Luciferase Reporter Assay System (Promega, catalog code TM040). Smad signaling activity was measured in *Mkl2*$^{-/-}$ ES cells using Cignal SMAD Reporter Kit (Qiagen, catalog code CCS-017L). All experiments were performed with duplicate plates of cells run in triplicate for each time point. Data are expressed as mean relative luciferase activity±s.e.m.

Chromatin immunoprecipitation analyses

Chromatin immunoprecipitation (ChIP) assays were performed with DNA harvested from wild-type and *Mkl2*$^{-/-}$ ES cells using a ChIP assay kit according to the manufacturer's directions (Millipore, catalog code 17-295). Polyclonal anti-SRF IgG (Santa Cruz, catalog code Sc335) or control rabbit IgG was used to immunoprecipitate cross-linked chromatin. Quantitative PCR was performed with Power SYBR Green PCR Mastermix and the PRISM 7500 (ABI). The nucleotide sequence of PCR primers used to amplify *Tgfβ2* CArG boxes 1-5 are shown in supplementary material Table S1.

Cell adhesion assays

Cell adhesion assays were performed using the Vybrant Cell Adhesion Assay kit (Invitrogen, cat. V-13181). ES cells (5×10^6/ml) were grown in 0.5% fetal bovine serum for 2 hours and then stained with calcein-AM. Following 1 hour of incubation on plastic or fibronectin-coated tissue culture wells, the fluorescence intensity (O.D.) of each well was measured. The percentage of adherent cells was determined by dividing the fluorescence intensity (O.D.) by the total fluorescence intensity of adherent cells in each well. Each experiment was repeated at least three times. Data are reported as the mean percentage of adherent cells±s.e.m.

Statistical analyses

Statistical significance was determined using the Student's *t*-test: $*P<0.05$; $**P<0.01$. For GSEA, significance of pathway enrichment in the setting of multiple comparisons was assessed using false discovery rate q-values as previously described (Subramanian et al., 2005). For ChIP analyses, statistical significance was determined with a one-way ANOVA test.

RESULTS

Mkl2$^{-/-}$ null mutant mice survive only until E13.5

Heterozygous *Mkl2* (*Mkl2*$^{+/-}$) mice were generated in which exon 8 was deleted, rendering the protein functionally null (supplementary material Fig. S1) (Wang et al., 2002). *Mkl2*$^{-/-}$ embryos survive until E13.5, but die between E13.5 and E16.5 (Table 1). At E15.5, fewer than 10% of the anticipated *Mkl2*$^{-/-}$ mutants survived and no viable *Mkl2*$^{-/-}$ embryos were observed beyond E16.5. Of note, the timing of embryonic demise is earlier than we observed in *Mkl2* gene trap mutants that exhibit a hypomorphic phenotype and survive until postnatal day (P) 1-2 (Li et al., 2005). Consistent with previous reports (Li et al., 2005; Oh et al., 2005), cardiac outflow tract patterning defects were observed in E14.5-16.5 *Mkl2*$^{-/-}$ embryos (data not shown). However, these defects failed to explain lethality at E13.5-16.5, which is prior to the transition from the fetal to the adult circulation that occurs in the immediate postnatal period.

Mkl2 null embryos develop arterial aneurysms and hemorrhage

Analyses of 859 embryos revealed that through E10.5, wild-type (*Mkl2*$^{+/+}$), heterozygous (*Mkl2*$^{+/-}$) and null (*Mkl2*$^{-/-}$) embryos were grossly indistinguishable. However, as early as E11.5, prior to aorticopulmonary septation, some *Mkl2*$^{-/-}$ embryos exhibited areas of focal hemorrhage. By E12.5, all *Mkl2*$^{-/-}$ mutants displayed regions of hemorrhage and all surviving E15.5 mutant embryos displayed large areas of hemorrhage covering their bodies (Fig. 1A,B). Histological analyses revealed dilation of the midline derivative of the ventral aorta (Ao) in all E11.0 *Mkl2*$^{-/-}$ embryos (Fig. 1C,D, white arrowheads). By E12.5, aneurysmal dilation (white arrows) of the aortic arch (Ao) (Fig. 1G,H) and 3rd pharyngeal arch artery (3PA) (Fig. 1E,F) was commonly observed in *Mkl2*$^{-/-}$ embryos. Aneurysmal dilation and arterial rupture (black arrows) was also observed in other arteries supplying the head and neck of *Mkl2*$^{-/-}$ embryos (Fig. 1F, arrows). In mutant embryos that survived to E15.5, massive aneurysmal dilation of the common carotid artery (CCA) was observed displacing the trachea (Tr) and esophagus (Es) (Fig. 1I,J). In addition, intraparenchymal hemorrhage of the embryonic liver and lung (white arrows) was observed in E12.5-15.5 *Mkl2*$^{-/-}$ mutant embryos (Fig. 1K,L). Taken together, these data suggest strongly that hemorrhage attributable to defects in select arteries contributed to the demise of *Mkl2*$^{-/-}$ embryos.

Disruption of the tunica media and structural integrity of *Mkl2*$^{-/-}$ arteries

Striking defects in the structural organization of the tunica media was observed in E12.5-15.5 *Mkl2*$^{-/-}$ arteries. In E12.5 *Mkl2*$^{-/-}$ embryos, the aortic sac (Ao) had enlarged and expanded rostrally into the neck beyond the level normally occupied by the 6th pharyngeal arch artery (Fig. 2A,B). The tunica media of the mutant aorta was thickened in some sections and reduced to a single layer of cells (arrow) in other sections (Fig. 2C,D). At E15.5, SMCs populating the aortic arch of control embryos are distinguished by their spindle-like morphology (arrows) and layered structure (Fig.

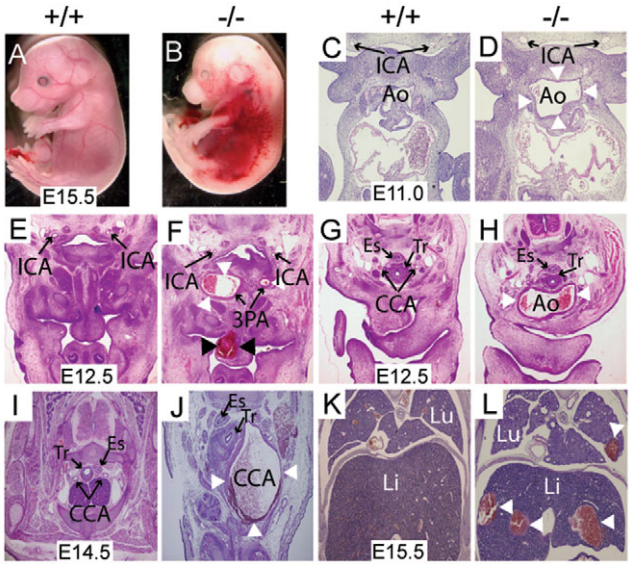

Fig. 1. *Mkl2*$^{-/-}$ embryos exhibit hemorrhage and aneurysmal dilation of the great arteries. (**A**,**B**) E15.5 wild-type (+/+) and *Mkl2*$^{-/-}$ (–/–) embryos demonstrating diffuse hemorrhage in the E15.5 mutant embryo. (**C**,**D**) Hematoxylin and Eosin-stained transverse sections of E11.0 wild-type and *Mkl2*$^{-/-}$ embryo, demonstrating dilated aortic sac (Ao) (arrowheads) in the mutant embryo. Original magnification was ×20. ICA, internal carotid artery. (**E**,**F**) Hematoxylin and Eosin-stained transverse section of E12.5 wild-type and *Mkl2*$^{-/-}$ embryo, demonstrating dilation of the 3rd PA artery and dilation and hemorrhage (black arrowheads) of the lingual vessels in the *Mkl2*$^{-/-}$ mutant embryo. Original magnification was ×20. White arrowheads indicate aneurysm. (**G**,**H**) Hematoxylin and Eosin-stained section of E12.5 wild-type and *Mkl2*$^{-/-}$ embryo, showing dilation of the mutant aorta (Ao, white arrowheads) extending to the level of the common carotid artery (CCA). Original magnification was ×20. ES, esophagus; Tr, trachea. (**I**,**J**) Hematoxylin and Eosin-stained transverse section of E14.5 wild-type and *Mkl2*$^{-/-}$ embryo, demonstrating aneurysmal dilation of the mutant common carotid artery (CCA). Original magnification was ×20. Arrowheads indicate aneurysm. (**K**,**L**) Hematoxylin and Eosin-stained frontal sections of E15.5 wild-type and *Mkl2*$^{-/-}$ embryos showing intra-parenchymal hemorrhages (white arrowheads) in the liver (Li) and lung (Lu) of the mutant embryo. Original magnification was ×20.

Table 1. Genotype analysis of embryos harvested from *Mkl2*$^{+/-}$ × *Mkl2*$^{+/-}$ staged matings

Age	*Mkl2*$^{+/+}$ (wild type)	*Mkl2*$^{+/-}$ (heterozygous)	*Mkl2*$^{-/-}$ (null)
E9.5	6	22	13 (20%)
E10.5	14	32	11 (17%)
E11.5	38	90	40 (22%)
E12.5	45	82	48 (29%)
E13.5	28	57	12* (10%)
E14.5	33	60	12* (10%)
E15.5	36	73	3* (2%)
E16.5	32	69	3* (2%)
P0	33	71	0

*Embryos undergoing resorption were genotyped.

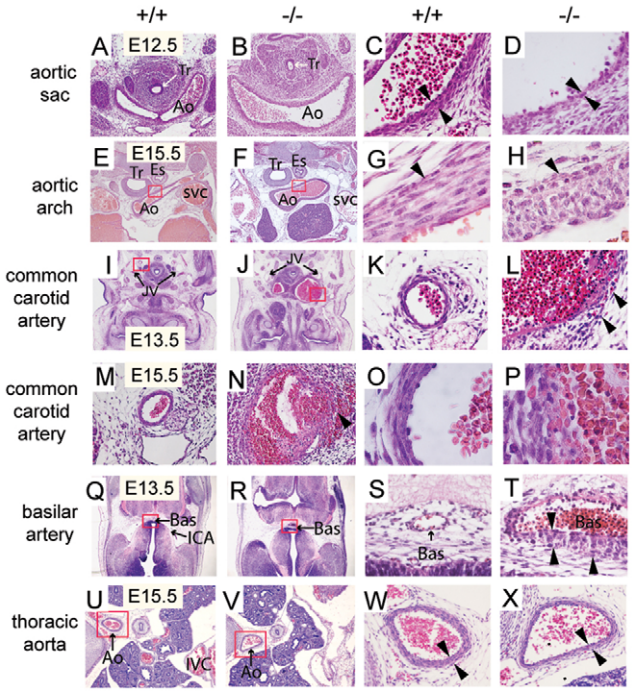

Fig. 2. Disruption of the tunica media and aneurysm formation in *Mkl2*$^{-/-}$ embryos. (**A-D**) Hematoxylin and Eosin-stained transverse section of E12.5 wild-type (+/+) and *Mkl2*$^{-/-}$ (–/–) embryos, demonstrating dilation of the mutant aortic sac in the *Mkl2*$^{-/-}$ mutant aorta (Ao). Tr, trachea. (**C**,**D**) High-power magnification of the wall of the aortic sac reveals thinning of the tunica media to a single layer of cells (arrowheads) in some segments of the *Mkl2*$^{-/-}$ mutant aortic sac. Original magnifications were ×100 (A,B) and ×400 (C,D). Tr, trachea. (**E-H**) Hematoxylin and Eosin-stained transverse section of the aortic arch (Ao) of E15.5 wild-type and *Mkl2*$^{-/-}$ embryo, demonstrating dilation of mutant aorta arch (Ao). The red rectangles in E and F indicate the locations of G and H. (G,H) High-power magnification of the tunica media (arrowhead) of the control artery reveals spindle-shaped SMCs oriented circumferentially (G); by contrast, medial SMCs populating the mutant artery appear polygonal lacking predominant orientation with obvious gaps between cells (H). Original magnifications were ×40 (E,F) and ×1000 (G,H). (**I-L**) Hematoxylin and Eosin-stained transverse section demonstrating aneurysmal dilation of the common carotid arteries of E13.5 wild-type and *Mkl2*$^{-/-}$ embryos. The location of the jugular vein (JV) is indicated. The red rectangles indicate the locations of K and L. (K,L) High-power magnification reveals thinning of the tunica media and rupture through the arterial wall (arrowheads) of the in the *Mkl2*$^{-/-}$ embryo (L). By contrast, spindle-like SMCs compose the media of the control artery (K). Original magnifications were ×20 (I,J) and ×200 (K,L). (**M-P**) Hematoxylin and Eosin-stained section showing the common carotid artery of E15.5 wild-type and *Mkl2*$^{-/-}$ embryo, demonstrating aneurysmal dilation, dissection and rupture (arrowhead) in the *Mkl2*$^{-/-}$ embryo (N). (O,P) High-power magnification demonstrates alignment of spindle-shaped SMCs surrounding the lumen of the control carotid artery (O). By contrast, SMCs of the *Mkl2*$^{-/-}$ artery are polygonal, lacking predominant orientation with intramural hemorrhage observed between cells (P). Original magnifications were ×100 (M,N) and ×1000 (O,P). (**Q-T**) Hematoxylin and Eosin-stained section of the basilar artery (Bas) of E13.5 wild-type and *Mkl2*$^{-/-}$ embryos demonstrating dilation of the mutant basilar artery (Bas) (R,T). The red rectangles in Q and R indicate the locations of S and T. (S,T) High-power magnification reveals disorganization of the tunica media (arrowheads) in the *Mkl2*$^{-/-}$ artery compared with the control basilar artery, which comprises a single layer of SMCs. Original magnifications were ×40 (Q,R) and ×400 (S,T). ICA, internal carotid artery. (**U-X**) Hematoxylin and Eosin-stained section showing the descending thoracic aorta of E15.5 wild-type (U,W) and *Mkl2*$^{-/-}$ (V,X) embryos. The red rectangles in U and V indicate the locations of W and X. Slight thinning of the tunica media (arrowheads) is observed in the *Mkl2*$^{-/-}$ mutant artery (X) compared with the control aorta (W). Original magnifications were ×40 (U,V) and ×200 (W,X). IVC, inferior vena cava. See also supplementary material Fig. S2.

2E,G). By contrast, the tunica media of *Mkl2*$^{-/-}$ embryos was populated with rounded heterogeneous cells lacking a predominant orientation with obvious gaps appearing between cells (Fig. 2F,H). Disruption of the tunica media was even more striking in the common carotid arteries (CCA) of E13.5-15.5 *Mkl2*$^{-/-}$ embryos (Fig. 2I-P). At E13.5, aneurysmal dilation, dissection and rupture (arrow) of the CCA was commonly observed in *Mkl2*$^{-/-}$ embryos (Fig. 2J,L). By contrast, three or four layers of circumferentially oriented vascular SMCs comprise the tunica media of wild-type littermates (Fig. 2I,K). Immunostaining with anti-tropoelastin antibody demonstrates disruption of cell-cell and cell-matrix relationships in *Mkl2*$^{-/-}$ carotid arteries compared with controls (supplementary material Fig. S2). Complex aneurysm formation and dissection with formation of a neointima that recapitulated pathological changes observed in humans was commonly observed in E15.5 *Mkl2*$^{-/-}$ carotid arteries (Fig. 2M-P). At E15.5, the tunica media of the carotid artery in wild-type embryos consists of four or five layers of well-organized, spindle-shaped SMCs (Fig. 2M,O). By contrast, gaps in the tunica media with penetrating hemorrhage (arrow) were observed in *Mkl2*$^{-/-}$ embryos and both medial and neointimal vascular SMCs were characterized by marked heterogeneity in size and orientation (Fig. 2N,P).

Inspection of the cerebral vasculature revealed dilation of the basilar artery in *Mkl2*$^{-/-}$ embryos compared with controls (Fig. 2Q-T). At E13.5, the lumen of the basilar (Bas) artery is typically surrounded by a single layer of circumferentially oriented SMA-positive vascular SMCs (Fig. 2Q,R). However, the basilar artery of *Mkl2*$^{-/-}$ mutants was markedly dilated and the lumen was surrounded by multiple layers of heterogeneous appearing cells (arrowheads) expressing SMC markers (Fig. 2S,T; supplementary material Fig. S5). Of note, SMCs contributing to the basilar artery are not derived from the cardiac neural crest. By contrast, only subtle differences were also observed in the descending thoracic aorta of E15.5 *Mkl2*$^{-/-}$ mutant compared with control littermates (Fig. 2U-X). In mutant embryos, the lumen of the thoracic aorta appeared eccentric with some thinning of the tunica media (arrows) compared with control littermates (Fig. 2V,X). Moreover, no obvious changes were observed in the iliac or femoral arteries of *Mkl2*$^{-/-}$ and control littermates. However, intra-parenchymal hemorrhage (white arrows) of the liver (Li) and lung (Lu) was commonly observed in E12.5-15.5 *Mkl2*$^{-/-}$ embryos (Fig. 1L). Taken together, these data demonstrate that the hemorrhage observed in *Mkl2*$^{-/-}$ embryos is attributable to defects in the structural integrity of select arteries owing to alterations in medial SMC morphology, orientation, and cell-cell and cell-ECM relationships.

MKL2 regulates TGFβ signaling in embryonic stem cells

Microarray analyses were performed with mRNA harvested from undifferentiated *Mkl2*$^{-/-}$ embryonic stem (ES) cells and from the parental wild-type SV129 ES cell line. We chose to compare

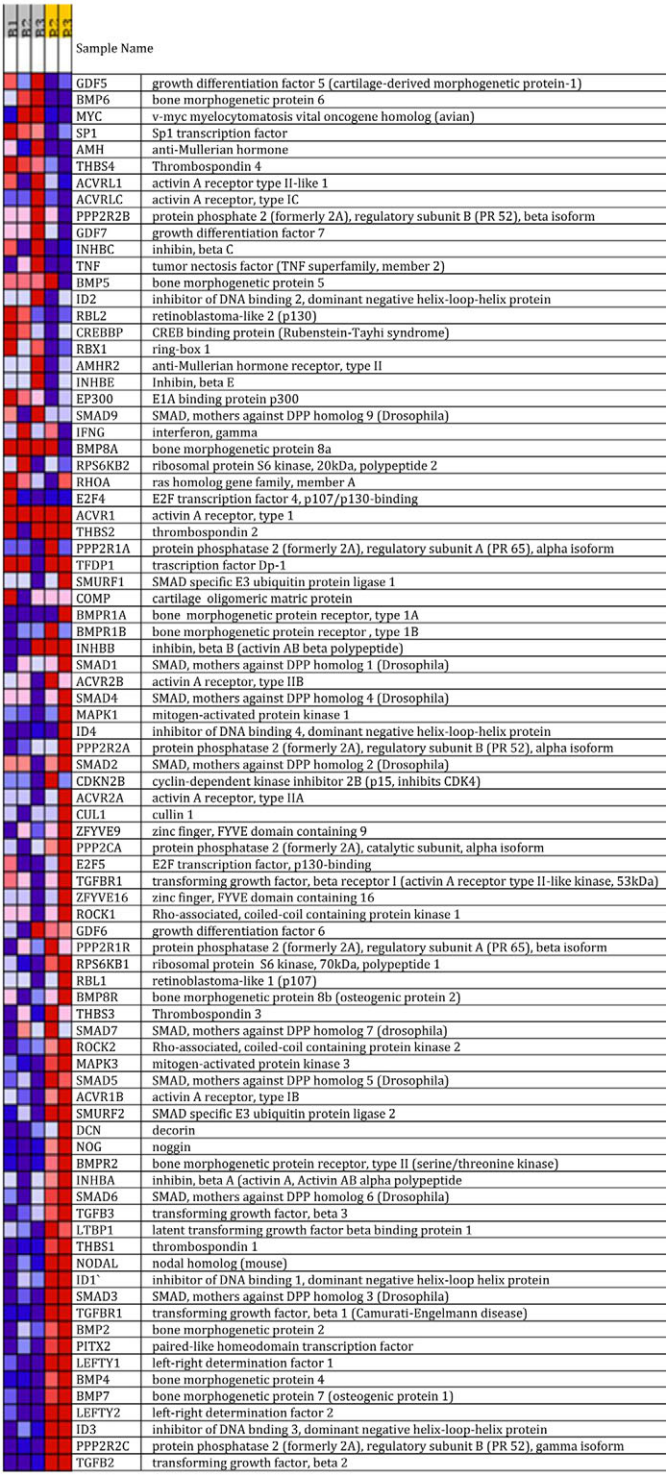

Fig. 3. Microarray analysis reveals reduced expression of TGFβ signaling pathway genes in *Mkl2*$^{-/-}$ ES cells. Microarray analysis was performed with mRNA harvested from undifferentiated wild-type and *Mkl2*$^{-/-}$ ES cells. To screen for pathways affected by *Mkl2* deletion, Gene Set Enrichment Analysis (GSEA) was applied to identify KEGG-designated signaling pathways that are coordinately induced or repressed in response to *Mkl2* deletion. The most repressed pathway was TGFβ signaling (FDR q value<0.0001). The heat map shown on the left displays the list of KEGG-designated genes in the TGFβ signaling pathway and their relative level of gene expression in biological replicate samples of *Mkl2*$^{-/-}$ (gray) and wild-type (yellow) ES cells. Red or blue signal indicates increased or decreased expression, respectively. Brightness is proportional to the difference from the median expression level. The NCBI gene identification names are listed on the right (see also Dünker and Krieglstein, 2002).

undifferentiated *Mkl2*$^{-/-}$ ES cells with control ES cells to identify MKL 2-regulated pathways that underlie basic developmental programs and to maximize signal-to-noise in the first stage of these analyses. These data were deposited in the Gene Expression Omnibus (GEO) public database (Accession Number GSE38316). In exploratory analyses, more genes were downregulated than upregulated in response to *Mkl2* deletion, consistent with the function of MKL2 as a transcriptional co-activator (supplementary material Table S3). To screen for canonical molecular pathways regulated directly or indirectly by *Mkl2* deletion, Gene Set Enrichment Analysis (GSEA) was applied to the microarray data. Remarkably, no Kyoto Encyclopedia of Genes and Genomes (KEGG)-defined molecular pathway was upregulated in *Mkl2*$^{-/-}$ ES cells compared with wild-type cells, whereas 55 KEGG-defined pathways showed evidence of repression (FDR q value<0.05; supplementary material Table S4). The most repressed pathway was TGFβ signaling, which showed substantial repression in multiple transcripts, including both TGFβ2 and TGFβ3 (FDR q value<0.0001) (Fig. 3). As shown in the heat map, TGFβ2 demonstrated the largest relative decrease in *Mkl2*$^{-/-}$ ES cells compared with wild-type ES cells (Fig. 3). qRT-PCR analysis confirmed an 84% reduction in undifferentiated TGFβ2 mRNA in *Mkl2*$^{-/-}$ ES cells compared with wild-type ES cells (supplementary material Fig. S3). Moreover, consistent with the microarray analysis, a 62% decrease in TGFβ3 mRNA was observed in *Mkl2*$^{-/-}$ ES cells (supplementary material Fig. S3). By contrast, a small, but statistically insignificant, difference was observed in TGFβ1 mRNA (supplementary material Fig. S3). However, expression of multiple other genes in the TGFβ signaling pathway was decreased in *Mkl2*$^{-/-}$ ES cells, including *Tgfbr1*, *Smad3*, *Ltbp1*, *Tgfb3*, *Smad6*, *Smad5*, *Smad7*, *Smad2*, *Smad4* and *Smad1* (Fig. 3). In addition, expression of multiple genes involved in the BMP signaling pathway were decreased in *Mkl2*$^{-/-}$ ES cells compared with the parental ES cell line, including *Bmp7*, *Bmp4*, *Bmp2*, *Inhba*, *Bmpr2*, *Acvrib*, *Bmp8r*, *Acvr2a*, *Acvr2b*, *Inhbb*, *Bmpr1b* and *Bmpr1a* (Fig. 3). These microarray findings were validated by qRT-PCR performed with mRNA harvested from *Mkl2*$^{-/-}$ ES cells and the parental ES cell line (supplementary material Fig. S3).

To determine whether TGFβ signaling was regulated during the differentiation of ES cells into cystic embryoid bodies, qRT-PCR was performed with mRNA harvested from *Mkl2*$^{-/-}$ and control ES cells after their differentiation into embryoid bodies (Fig. 4A). As anticipated, *Mkl2* gene expression was below the limits of detection in *Mkl2*$^{-/-}$ ES cells, but the *Mkl2* gene was expressed abundantly in wild-type ES cells (Fig. 4A,B) (P<0.01). No significant difference was observed in MKL1 and SRF mRNA in wild-type and *Mkl2*$^{-/-}$ ES cells (Fig. 4A,B). Once again, *Tgfb2* gene expression was decreased by 84.0±3.4% in *Mkl2*$^{-/-}$ ES cell compared with control cells (Fig. 4A,B) (P<0.01). Of note, TGFβ2 mRNA was also reduced in differentiating *Srf*$^{-/-}$ ES cells (Fig. 4B). In addition, expression of TGFβ1 and TGFβ3 mRNA was reduced to 65.0±16.3% and 45.3±5.5%, respectively, in differentiating

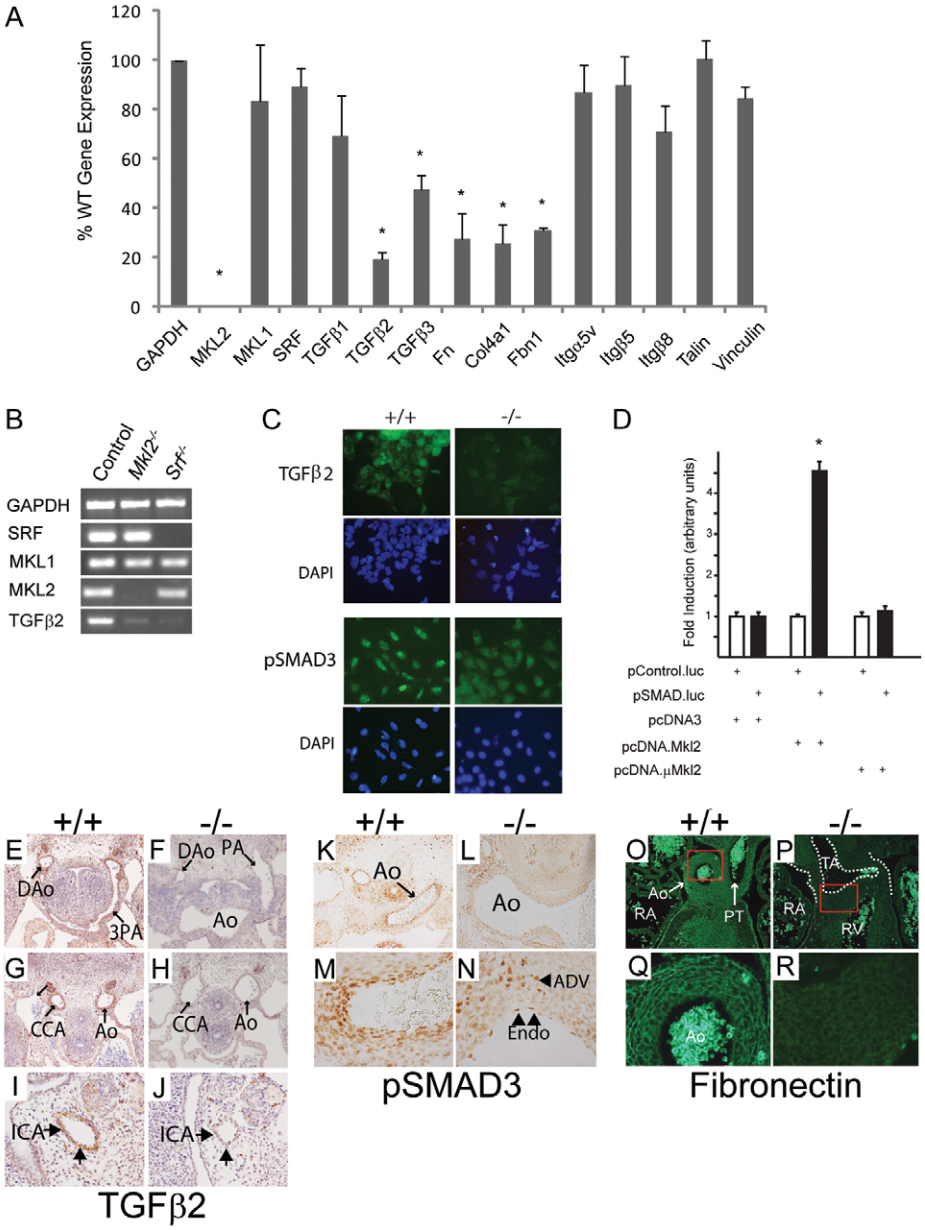

Fig. 4. TGFβ signaling is downregulated in *Mkl2*$^{-/-}$ ES cells and the great arteries of *Mkl2*$^{-/-}$ embryos. (**A**) qRT-PCR analyses performed with mRNA harvested from wild-type and *Mkl2*$^{-/-}$ ES cells following 6 days of differentiation in vitro. The experiment was performed three times with three biological replicates used in each experiment. Data are expressed as the percentage of wild-type gene expression observed in *Mkl2*$^{-/-}$ ES cells±s.e.m. (*P<0.01 versus wild-type gene expression). (**B**) A representative ethidium bromide-stained agarose gel showing amplified RT-PCR products obtained with mRNA harvested from wild-type (control), *Mkl2*$^{-/-}$ and *Srf*$^{-/-}$ ES cells and PCR primers that amplify GAPDH, SRF, MKL1, MKL2 and TGFβ2 mRNA. (**C**) Photomicrograph showing differentiating wild-type (+/+) and *Mkl2*$^{-/-}$ (–/–) ES cells plated on fibronectin-coated plates immunostained with anti-TGFβ2 antibody (green stain), anti-phospho-SMAD3 (pSMAD3) antibody (green) or DAPI counterstain (blue nuclear stain). Original magnification was ×400. (**D**) Transient co-transfection analyses was performed with *Mkl2*$^{-/-}$ ES cells co-transfected with the pSMAD.luc reporter plasmid (black bars) or the pControl.luc plasmid (white bars) and expression plasmids encoding MKL2 (pcDNA.MKL2), a dominant-negative μMKL2 mutant protein (pcDNAμMKL2) or the negative control plasmid pcDNA3, respectively. Data are expressed as the fold induction in luciferase activity (arbitrary units) compared with luciferase activity observed in cells co-transfected with the pControl.luc reporter plasmid±s.e.m. (*P<0.001). (**E-J**) Transverse sections harvested from E12.5 wild-type (+/+) and *Mkl2*$^{-/-}$ (–/–) embryos immunostained with anti-TGFβ2 antibody (brown). The dorsal aorta (DAo), pharyngeal arch arteries (PA), aorta (Ao), common carotid artery (CCA) and internal carotid artery (ICA) are identified. Original magnifications were ×100 (E-H) and ×200 (I,J). Arrows in I,J indicate TGFβ2 expression. (**K-N**) Transverse sections showing the aortic arch (Ao) of E12.5 wild-type (K,M) and *Mkl2*$^{-/-}$ (L,N) embryos immunostained with anti-phospho-SMAD3 antibody (brown). (L,N) High-power magnification reveals abundant nuclear phospho-SMAD-3 in endothelial cells (Endo) and adventitial (ADV) cells of *Mkl2*$^{-/-}$aorta, whereas pSMAD3 expression is markedly attenuated in medial SMCs. Original magnifications were ×100 (K,L) and ×400 (M,N). (**O-R**) Cardiac outflow tract of E14.5 wild-type (O,Q) and *Mkl2*$^{-/-}$ (P,R) embryos immunostained with anti-fibronectin antibody. The red rectangles in O and Q indicate the regions shown in P and R. Abundant fibronectin (green) is observed throughout the ascending aorta (Ao) and pulmonary trunk (PT) of the wild-type embryo (O,P). By contrast, expression of fibronectin is markedly attenuated throughout the mutant truncus arteriosus (TA) of the *Mkl2*$^{-/-}$ embryo (Q,R). RA, right atria; RV, right ventricle. Original magnifications were ×100 (I,K) and ×400 (J,L).

Mkl2$^{-/-}$ ES cells compared with control cells (Fig. 4A) (P<0.01). Moreover, TGFβ-regulated genes encoding extracellular matrix (ECM) were downregulated in differentiating *Mkl2*$^{-/-}$ ES cells. Fibronectin (Fn) exhibited a 77.3±10.1% decrease, type IV collagen α1 (Col4a1) exhibited a 78.5±7.4% decrease and fibrillin 1 (*Fbn1*) exhibited a 75.8±1.0% decrease compared with wild-type ES cells (Fig. 4A) (P<0.01). By contrast, integrins αV, β8 and β5, as well as the vinculin and talin genes were expressed at comparable levels in *Mkl2*$^{-/-}$ and wild-type ES cells (Fig. 4A).

Consistent with these findings, abundant expression of TGFβ2 protein (green stain) was observed in differentiating wild-type ES cells, whereas TGFβ2 protein was not detected above background levels in *Mkl2*$^{-/-}$ ES cells (Fig. 4C). Moreover, TGFβ signaling, as assessed by the nuclear accumulation of phosphorylated Smad3, was dramatically downregulated in differentiating *Mkl2*$^{-/-}$ ES cells compared with wild-type ES cells (Fig. 4C). Co-transfection of *Mkl2*$^{-/-}$ ES cells with the pSMAD.luc luciferase reporter plasmid and an expression plasmid encoding mouse MKL2 revealed a 4.5-fold increase in luciferase reporter plasmid above levels observed in *Mkl2*$^{-/-}$ ES cells co-transfected with pSMAD.luc and pcDNA3 alone (P<0.01) (Fig. 4D). As anticipated, MKL2 failed to transactivate the negative control luciferase reporter plasmid pControl.luc and forced expression of the dominant-negative MKL2 mutant protein failed to transactivate the pSMAD.luc reporter plasmid (Fig. 4D). Taken together, these data demonstrate that MKL2 regulates TGFβ2 gene expression, TGFβ signaling and a subset of TGFβ responsive genes encoding ECM in ES cells.

Mkl2$^{-/-}$ mutants exhibit a block in TGFβ signaling in the embryonic vasculature

Consistent with previous reports (Molin et al., 2003), low, but detectable, levels of TGFβ3 (green stain) were observed in the cardiac outflow tract and great arteries at this stage of embryonic development (supplementary material Fig. S4A,B,E,F). At the level of sensitivity afforded by immunohistochemistry, no obvious difference in TGFβ1 or TGFβ3 expression was observed in the cardiac outflow tract and great arteries of *Mkl2*$^{-/-}$ embryos compared with wild-type littermates (supplementary material Fig. S4C,D,G,H). By contrast, abundant TGFβ2 (brown stain) was observed in the great arteries, including the right dorsal aorta (DAo), 3rd pharyngeal arch artery (3PA), common carotid artery (CCA), aorta (Ao) and internal carotid artery (ICA) of wild-type embryos (Fig. 4E,G,I). By contrast, TGFβ2 expression was markedly attenuated in the great arteries of *Mkl2*$^{-/-}$ embryos (Fig. 4F,H,J). Consistent with these observations, the nuclear accumulation of phosphorylated Smad3 (brown stain) was dramatically downregulated in the tunica media of the aorta (Ao) and great arteries in E13.5 *Mkl2*$^{-/-}$ mutant embryos (Fig. 4K-N; data not shown). By contrast, comparable levels of TGFβ2 were observed in intimal endothelial cells (End) and adventitial (ADV) cells in the control and mutant embryos (compare Fig. 4M,N). Moreover, fibronectin (green stain) was dramatically downregulated in the ascending aorta (Ao) and great arteries of E14.5 *Mkl2*$^{-/-}$ embryos compared with control littermates (Fig. 4O,P). In wild-type embryos, fibronectin is expressed throughout the media of the aorta (Ao) and pulmonary trunk (PT) (Fig. 4O,P). By contrast, very low levels of fibronectin were observed in the media of the mutant truncus arteriosus (TA) (Fig. 4Q,R). Taken together, these data demonstrate that, as in ES cells, TGFβ2 expression, TGFβ signaling and expression of the TGFβ-regulated gene fibronectin are downregulated in the great arteries of *Mkl2*$^{-/-}$ embryos.

The TGFβ2 gene is a direct transcriptional target of MKL2

A bioinformatics search revealed five putative SRF-bindings sites, or CArG boxes, in the mouse TGFβ2 promoter and intron sequences, including a consensus CArG box at –1491 bp (Fig. 5A; data not shown). In addition, eight putative CArG boxes were identified within, or flanking, the human *Tgfb2* gene (Fig. 5A; data not shown). Moreover, five CArG boxes (four consensus) were identified within, or flanking, the zebrafish *Tgfb2* gene (Fig. 5A; data not shown). Transient co-transfection analyses of Cos-7 cells with increasing concentrations of an expression plasmid encoding mouse MKL2 (pcDNA.MKL2) and the pTGFβ2Pr.luc reporter plasmid, which is under the control of the 1.7-k murine TGFβ2 promoter, revealed a stepwise increase in luciferase activity up to 31-fold higher than levels observed when cells were co-transfected with pcDNA3 and pTGFβ2Pr.luc (Fig. 5B). By contrast, a fivefold increase in luciferase activity was observed when Cos-7 cells were co-transfected with pcDNA.MKL2 and the pTGFβ2 μCARG.luc reporter plasmid, indicating that most, but not all, MKL2-mediated transcriptional activity is dependent upon CArG box 1 in the TGFβ2 promoter (Fig. 5B). In addition, forced expression of MKL2 in Cos-7 cells transactivated the TGFβ2 promoter 4.7-fold higher than levels observed in cells co-transfected with the pcDNA3 control expression plasmid (Fig. 5C). Surprisingly, however, co-transfection with expression plasmids encoding MKL1 or myocardin failed to increase luciferase activities above levels observed when cells were co-transfected with pcDNA3 (Fig. 5C). As anticipated, forced expression of the dominant-negative MKL2 mutant protein did not transactivate the TGFβ2 promoter (Fig. 5C).

Next, to determine whether an MKL2/SRF protein complex binds directly to one or more of the CArG boxes in the mouse *Tgfb2* gene in vivo, chromatin immunoprecipitation (ChIP) analyses were performed (Fig. 5D). Remarkably, 15-fold enrichment of immunoprecipitated, amplified SRF bound to CArG box 1 (CArG1) DNA was observed in wild-type ES cells (P<0.01) (Fig. 5D, dark gray bars). By contrast, in *Mkl2*$^{-/-}$ ES cells (Fig. 5D, light gray bars), only a two-fold increase in SRF bound to CArG box 1 was observed, demonstrating that binding of SRF to CArG box1 is dependent upon MKL2. Surprisingly, however, a less than two-fold enrichment of immunoprecipitated SRF bound to DNA was observed with PCR primers flanking CArG boxes 2-5, respectively, in wild-type and *Mkl2*$^{-/-}$ ES cells: a difference which was not statistically significant (Fig. 5D). Taken together, these data demonstrate that transcription of the *Tgfb2* gene is activated via binding of an MKL2/SRF protein complex to CArG box 1 of the mouse TGFβ2 promoter.

Mkl2$^{-/-}$ ES cells exhibit defects in cytoskeletal organization and cell adhesion

Attempts to grow *Mkl2*$^{-/-}$ ES cells were hindered because the cells failed to adhere to uncoated tissue culture plates. To overcome this problem, *Mkl2*$^{-/-}$ ES cells were grown on plates coated with fibronectin. Phase-contrast microscopy revealed that, as they differentiate, wild-type ES cells adhere to fibronectin matrix, and spread and form numerous protrusive lamellpodia and filopodia (Fig. 6A,C, arrows). By contrast, the *Mkl2*$^{-/-}$ ES cells exhibited obvious defects in cell adhesion, maintaining a rounded appearance with rare protrusions (Fig. 6B,D). To better characterize cell morphology and adhesion, differentiating control and *Mkl2*$^{-/-}$ ES cells were plated on collagen and immunostained with a panel of antibodies that recognize proteins involved in cytoskeletal organization and cell adhesion (Fig. 6E-L). Six days after plating,

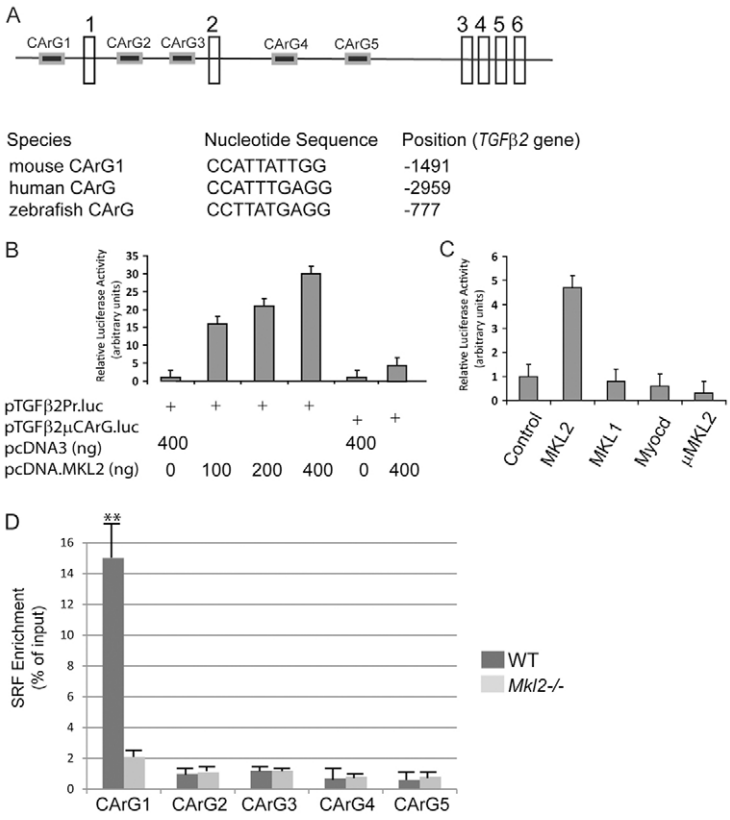

Fig. 5. The TGFβ2 promoter is activated by an Mkl2/Srf protein complex. (**A**) Schematic representation of the mouse *Tgfb2* gene showing location of the five CArG boxes (CArG1-5). The nucleotide sequence of CArG boxes identified in the mouse, human and zebrafish TGFβ2 promoters are shown. (**B**) Cos-7 cells were co-transfected with 400 ng (+) of the pTGFβ2Pr.luc reporter plasmid or the pTGFβ2 μCArG.luc reporter plasmid and the indicated amount (ng) of the pcDNA.Mkl2 expression plasmid encoding mouse MKL2. Data are expressed as relative luciferase activity (arbitrary units) compared with cells co-transfected with the control expression plasmid pcDNA3±s.e.m. (**C**) Cos-7 cells were co-transfected with pTGFβ2Pr.luc and expression plasmids encoding mouse MKL2, MKL1, myocardin and dominant-negative MKL2 mutant protein. Data are expressed as relative luciferase activity (arbitrary units) compared with cells co-transfected with pTGFβ2Pr.luc and pcDNA3±s.e.m. (**D**) Chromatin immunoprecipitation (ChIP) analyses performed with chromatin harvested from wild-type (dark-gray bars) and *Mkl2*$^{-/-}$ (light-gray bars) ES cells. Chromatin was immunoprecipitated with anti-SRF antibody and qPCR was performed with PCR primers that selectively amplify genomic DNA spanning CArG boxes 1-5, respectively, of the *Tgfb2* gene. Immunoprecipitated DNA was normalized to input DNA. Data are expressed as the mean SRF enrichment (% of input)±s.e.m. (n=4). $^{**}P$<0.01.

wild-type ES cells located on the margins of embryoid bodies spread and begin to migrate, demonstrating numerous lamellopodia and filopodia (Fig. 6A,C,E). By contrast, *Mkl2*$^{-/-}$ ES cells assumed a polygonal shape that rarely demonstrated lamellopodia or filopodia (Fig. 6B,D,F). Paxillin (pPax) (green stain), a component of focal adhesions, was observed in discrete complexes across the surface of wild-type ES cells (Fig. 6E, arrows). By contrast, relatively low levels of dot-like phosphorylated paxillin complexes were observed on the margins of *Mkl2*$^{-/-}$ ES cells (Fig. 6F). Wild-type ES cells exhibited dense F-actin networks (red stain) throughout their cytoplasm and at the leading edge of lamellopodium (Fig. 6G, arrows). By contrast, centrally located dot-like focal adhesions that are indicative of a less-motile cell were visualized in *Mkl2*$^{-/-}$ ES cells (Fig. 6H). DNase I staining revealed comparable expression of G-actin (green stain) in wild-type and *Mkl2*$^{-/-}$ ES cells, strongly suggesting that the F:G actin ratio is decreased in *Mkl2*$^{-/-}$ ES cells (Fig. 6I,J). Finally, discrete complexes containing fibronectin (Fn) were observed in wild-type ES cells, often localizing to lamellpodia and filopodia (Fig. 6K, arrows). By contrast, very low levels of fibronectin were observed in the perinuclear region of *Mkl2*$^{-/-}$ ES cells (Fig. 6L).

A quantitative fluorescence-based cell adhesion assay demonstrated that *Mkl2*$^{-/-}$ ES cells exhibit profound defects in cell adhesion to bovine serum albumin (BSA)-coated tissue culture plates. After 1 hour of incubation, 21.2±3.1% of wild-type (WT) cells adhere to the uncoated plates, whereas only 8.0±1.8% of *Mkl2*$^{-/-}$ ES cells adhere (P<0.001) (Fig. 6M). By contrast, 30.4±3.2% of wild-type ES cells and 33.7±1.9% of *Mkl2*$^{-/-}$ ES cells adhere to fibronectin-coated tissue culture plates, a difference that is not statistically significant (Fig. 6M). This suggested that the adhesive defects observed in *Mkl2*$^{-/-}$ ES cells were caused, at least in part, by a block in TGFβ2-induced expression of fibronectin. Consistent with this hypothesis, forced expression of TGFβ2 in *Mkl2*$^{-/-}$ ES cells restored the capacity of *Mkl2*$^{-/-}$ ES cells to adhere to BSA-coated tissue culture plates (8.0±1.8% versus 18.2±3.1%; P<0.001) (Fig. 6M). Of note, forced expression of TGFβ2 in *Mkl2*$^{-/-}$ ES cells enhanced the capacity of these cells to adhere to fibronectin-coated plates even beyond the capacity of wild-type ES cells (39.2±2.6% versus 30.4±3.4%; P<0.05).

To confirm that TGFβ2 did indeed induce expression of fibronectin in *Mkl2*$^{-/-}$ ES cells, two complementary assays were employed. Immunoblot analysis revealed a 51% decrease in expression of cellular fibronectin protein in *Mkl2*$^{-/-}$ ES cells compared with control cells (Fig. 6N). Similarly, *Srf*$^{-/-}$ ES cells exhibit a 63% decrease in expression of cellular fibronectin compared with wild-type ES cells (Fig. 6N). However, in *Mkl2*$^{-/-}$ ES cells stably transduced with an expression plasmid encoding TGFβ2, expression of cellular fibronectin was restored to levels approaching those observed in wild-type ES cells (Fig. 6N). Consistent with these findings, a quantitative radioimmunoassay revealed a 60% decrease in secreted fibronectin in the media of *Mkl2*$^{-/-}$ ES cells (16.2±0.5 ng/ml) compared with wild-type ES cells (40.5±1.0 ng/ml) (P<0.001) (Fig. 6O). Once again, forced expression of TGFβ2 in *Mkl2*$^{-/-}$ ES cells led to enhanced secretion of fibronectin (144.4±1.0 ng/ml) above levels observed in the media of wild-type ES cells (P<0.001) (Fig. 6O). Taken together, these data demonstrate that MKL2 activates transcription of the *Tgfb2* gene, which in turn activates expression of genes encoding TGFβ-regulated genes, including fibronectin, influencing the adhesive properties of the cell.

DISCUSSION

Transcriptional co-activators play crucial roles transducing signals that expand information encoded within the genome during

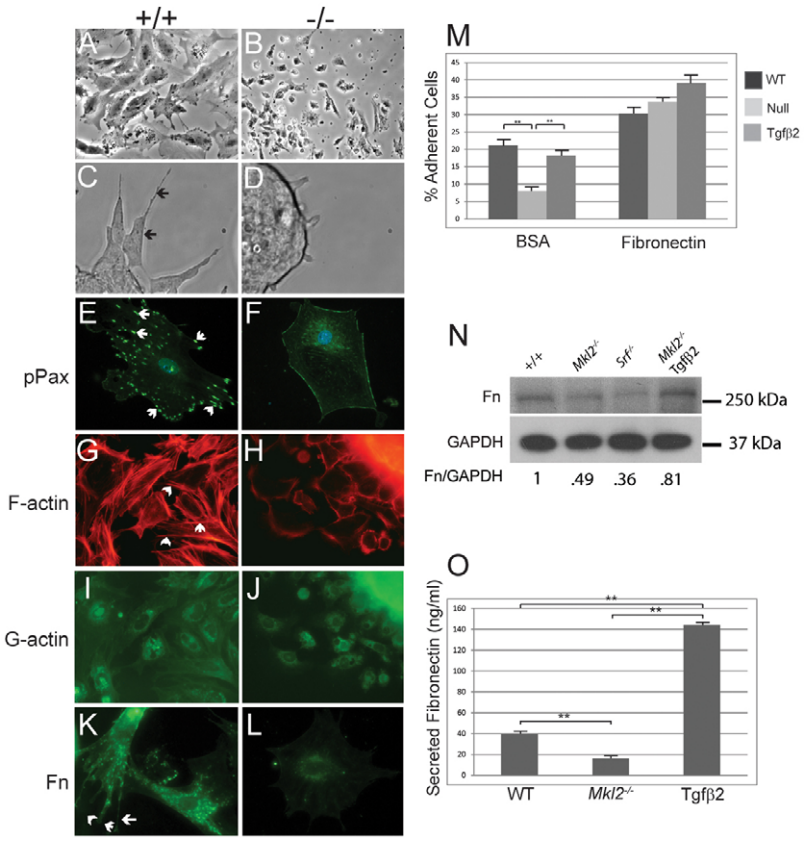

Fig. 6. *Mkl2*$^{-/-}$ ES cells exhibit derangements in cytoskeletal organization and cell adhesion that are rescued by TGFβ2. (**A-D**) Phase-contrast micrographs showing wild-type (A,C) and *Mkl2*$^{-/-}$ (B,D) ES cells 24 hours after plating on fibronectin-coated chamber slides. Wild-type ES cells spread and form numerous protrusive lamellpodia and filopodia (arrows) (C). Original magnifications were ×20 (A,B) and ×200 (C,D). (E-L) Immunostaining of wild-type and *Mkl2*$^{-/-}$ ES cells for expression of proteins associated with cell adhesion and cytoskeletal organization. (**E**,**F**) Wild-type and *Mkl2*$^{-/-}$ ES cells immunostained with anti-phospho-paxillin (green) and counterstained with DAPI (blue), demonstrating abundant expression in complexes across wild-type ES cells and low level expression at margins of *Mkl2*$^{-/-}$ ES cell. Arrows indicate focal adhesions. (**G**,**H**) Staining with rhodamine-phalloidin, which localizes to F-actin (red), demonstrates a rich array of actin filaments in control ES cells and absence of stress fibers in *Mkl2*$^{-/-}$ ES cells. Arrows indicate actin filaments. (**I**,**J**) ES cells were exposed to DNase I to identify monomeric G-actin (green). (**K**,**L**) ES cells immunostained with anti-fibronectin antibody demonstrate abundant expression in wild-type ES cells with localization to lamellopodia and filopodia (K, white arrows). By contrast, relatively low levels of fibronectin are observed in the perinuclear regions of *Mkl2*$^{-/-}$ ES cells (L). Original magnification ×400. (**M**) A fluorometric cell adhesion assay was performed comparing the capacity of wild-type (WT) ES cells (black bars), *Mkl2*$^{-/-}$ null ES cells (light-gray bars) and *Mkl2*$^{-/-}$ null ES cells stably transfected with an expression plasmid encoding TGFβ2 (gray bars) to adhere to BSA- or fibronectin-coated tissue culture plates. Data are expressed as % adherent cells±s.e.m. (**P<0.01). (**N**) Immunoblot analysis of fibronectin (Fn) expression in cell lysates prepared from wild-type (+/+) *Mkl2*$^{-/-}$, *Srf*$^{-/-}$ and *Mkl2*$^{-/-}$ + TGFβ2 ES cells, respectively. The fibronectin signal was normalized to expression of GAPDH (bottom panel). Data are expressed as normalized Fn expression compared with Fn expression in wild-type ES cells. MW standards are shown on the right of the blot. (**O**) An ELISA assay was employed to quantify secreted fibronectin in medium harvested from wild-type, *Mkl2*$^{-/-}$ and *Mkl2*$^{-/-}$ + TGFβ2 ES cells after 1 hour of incubation. Data are expressed as mean secreted fibronectin (ng/ml)±s.e.m. **P<0.001.

embryonic development and in response to environmental cues and signals. Our group and others have reported that *Mkl2* loss-of-function mutant embryos exhibit defects in vascular patterning attributable to a cell-autonomous block in differentiation of neural crest-derived vascular SMCs (Li et al., 2005; Oh et al., 2005; Wei et al., 2007). However, this defect fails to explain the lethality in *Mkl2*$^{-/-}$ embryos that occurs between E13.5 and E15.5. The studies described in this report demonstrate that *Mkl2*$^{-/-}$ embryos exhibit hemorrhage caused by aneurysmal dilation and dissection of select arterial beds throughout the embryo. Surprisingly, microarray studies and qRT-PCR experiments identified a conserved MKL2-regulated TGFβ signaling pathway in ES cells. Moreover, *Mkl2*$^{-/-}$ ES cells exhibit profound defects in cell adhesion that are rescued by forced expression of TGFβ2. Consistent with this observation, TGFβ2 expression, TGFβ signaling and TGFβ-regulated genes encoding key components of the ECM are downregulated in the developing vasculature of *Mkl2*$^{-/-}$ embryos.

The identification of an MKL2/TGFβ signaling pathway provides important new insights into the molecular mechanisms underlying MKL2/SRF function in the embryonic vasculature. As reported previously, an SRF/MKL2 complex plays a crucial role in activating a subset of SRF-dependent genes that encode SMC contractile proteins in neural crest-derived vascular SMCs (Li et al., 2005; Oh et al., 2005; Wei et al., 2007). Indeed, expression of SM-α-actin and SM-MyHC is severely attenuated in vascular SMCs populating the aorta and pharyngeal arch arteries in E12.5 *Mkl2*$^{-/-}$ embryos compared with wild-type (WT) littermates (supplementary material Fig. S5A-H). Surprisingly, in *Mkl2*$^{-/-}$

embryos expression of SM-MyHC and SM-α-actin is also dramatically downregulated in a subset of non-neural crest-derived vascular SMCs, including those populating the mutant basilar artery (supplementary material Fig. S5I,J) and hepatic vasculature (J.L., unpublished observations). These findings demonstrate that the role of MKL2 in the vasculature is not restricted to cardiac neural crest-derived SMCs. This raises the crucial issue of whether defects in vascular patterning and stabilization in the embryo resulted primarily from an MKL2-mediated block in expression of genes encoding contractile SMC proteins versus a block in TGFβ signaling. Indeed, mutations of the *ACTA2* gene are associated with familial thoracic aneurysms in humans (Guo et al., 2007; Morisaki et al., 2009; Regalado et al., 2011). However, it is noteworthy that conditional ablation of the myocardin (*Myocd*) gene in cardiac neural crest-derived SMCs results in dramatic suppression of the SMC contractile proteins that was not accompanied by vascular aneurysm, dissection or hemorrhage (Huang et al., 2008). Ultimately, as discussed below and shown in Fig. 7, we believe that MKL2/SRF-mediated loss of SMC contractile proteins in *Mkl2*$^{-/-}$ embryos directly contributes to the vascular phenotype observed in *Mkl2*$^{-/-}$ embryos and the loss of SMC contractile proteins indirectly influences TGFβ signaling in the vasculature. Conversely, TGFβ signaling, in turn, directly and indirectly influences the contractile SMC gene program. This model highlights the crucial role that the transcriptional co-activator MKL2 plays in regulating angiogenesis and vascular patterning in the embryo.

The data provided in this report expands our understanding of the function of MKL2 in the embryo by revealing that MKL2 lies upstream in a transcriptional program that regulates TGFβ expression, TGFβ signaling and TGFβ-regulated genes encoding ECM. Surprisingly, we observed that MKL2 profoundly influences the morphology and adhesive properties of ES cells that act at least in part via TGFβ/BMP signaling. As shown in Fig. 7, in the embryonic vasculature, developmental cues and extracellular signals transduced via RhoA and cytoskeletal actin promote the translocation of G-actin/MKL2 complexes from the cytoplasm to the SMC nucleus (Mouilleron et al., 2011). In the nucleus, MKL2 physically associates with SRF, which promotes the binding of the MKL2/SRF complex to the TGFβ2 promoter (and related TGFβ family members), activating TGFβ signaling in the arterial wall. TGFβ signaling, in turn, activates expression of a subset of genes encoding ECM, including fibronectin (*Fbn*), fibrillin 1 (*Fbn1*) and Col4a1 (*Col4a1*). The ECM feeds back upon the vascular SMC, modulating its structure, morphology, adhesive and migratory properties (Astrof and Hynes, 2009; Pardali et al., 2010). These new data support a model wherein the loss of MKL2 results in a block in TGFβ signaling in select arterial beds, including the great arteries, causing alterations in cell adhesion with disruption of the tunica media, which ultimately leads to aneurysmal dilation and hemorrhage. Consistent with this model, in E10.5 *EIIIA/EIIIB* fibronectin-double null embryos defective association of vascular SMCs with the endothelium of the aorta is observed. Interestingly, in fibronectin mutant embryos, vascular SMCs assume a rounded morphology resembling that observed in *Mkl2*$^{-/-}$ mutant embryos (Astrof et al., 2007). As such, these new data serve to identify a second arm (shown in red) of the MKL2 signaling pathway that plays a crucial role in regulating angiogenesis and vascular stabilization required for embryonic survival (Fig. 7).

Other data supporting this model include the overlapping patterns of MKL2 and TGFβ2 expression in the embryonic vasculature. Fate-mapping studies have shown that, in the E8.0 mouse embryo, MKL2 mRNA is observed in cardiac neural crest cells located in the hindbrain prior to their migration to the cardiac outflow tract and great arteries and MKL2 is expressed abundantly in these arteries throughout development (Li et al., 2005). Similarly, TGFβ2 is the predominant TGFβ isoform expressed in the great arteries and the gene is expressed abundantly in SMCs populating the aortic sac and pharyngeal arch arteries in a temporal window consistent with MKL2-induced activation of the *Tgfb2* gene (Molin et al., 2003). Therefore, it is not surprising that *Mkl2*$^{-/-}$

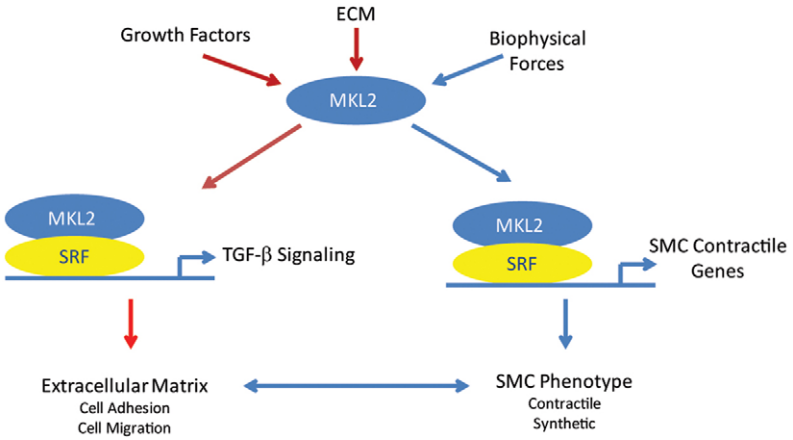

Fig. 7. An MKL2/TGFβ signaling pathway is required for vascular patterning and stabilization of the great arteries during embryonic development. The transcriptional co-activator MKL2 transduces multiple signals in vascular SMCs that promote translocation of MKL2 (bound to G-actin) to the nucleus, where it physically associates with SRF. This, in turn, promotes SRF binding to CArG boxes, which activates transcription of the *Tgfb2* gene and other genes encoding TGFβ signaling molecules. Activation of TGFβ signaling activates expression genes that encode key components of the ECM, including fibronectin, fibrillin and Col4a1. The ECM, in turn, feeds back on vascular SMCs, reinforcing the contractile SMC phenotype and leading to organization of the tunica media that is required for stabilization of the great arteries. In addition, MKL2 promotes SMC differentiation of the great arteries via binding to SRF, which in turn binds to CArG boxes that control expression of genes encoding SMC contractile proteins. Expression of SMC contractile proteins influences expression of TGFβ signaling and TGFβ-regulated genes encoding ECM, and visa versa, serving to define an MKL2/SRF molecular program required for vascular development and patterning in the embryo. Pathways identified in the experiments described in this work are shown in red.

and *Tgfb2*$^{-/-}$ embryos exhibit vascular defects that are attributable, at least in part, to a block of TGFβ signaling in aortic sac and the 4th pharyngeal arch artery, which gives rise to the aortic arch. Consistent with this observation, abundant nuclear Smad2 expression is observed in the 4th pharyngeal arch segment of the aortic arch, but not in other pharyngeal arch segments or the ascending or descending aorta (Molin et al., 2004). Similarly, fibronectin, a TGFβ target gene that is dramatically downregulated in *Mkl2*$^{-/-}$ ES cells and arteries, is expressed abundantly in the aortic sac and pharyngeal arch arteries. Therefore, vulnerability of the aorta and fourth pharyngeal arch arteries may be linked to a localized reduced vascular Smad2/3 signaling and related expression of fibronectin in *Mkl2*$^{-/-}$ embryos. The findings that TGFβ2, the predominant TGF-β isoform expressed in the cardiac outflow tract and great arteries in the embryo, as well as SMAD signaling and fibronectin are dramatically downregulated in the great arteries of *Mkl2*$^{-/-}$ embryos is consistent with this model. Taken together, these data support the conclusion that the vascular pathology observed in *Mkl2*$^{-/-}$ embryos results from a block in MKL2-induced expression of TGFβ2 (and probably TGFβ3) and TGFβ signaling in the developing arterial wall, reflecting the crucial role that SRF and MKL2 play in development of the aorta and great arteries in the embryo.

This raises the important question of how does the block in TGFβ signaling observed in ES cells relate to the vascular phenotype observed in *Mkl2*$^{-/-}$ mutant embryos? Remarkably, multiple genes encoding TGFβ/BMP signaling molecules were downregulated in undifferentiated *Mkl2*$^{-/-}$ ES cells (Fig. 3; Fig. 4A and supplementary material Fig. S3). Some, but not all, of these genes are expressed in the developing vasculature. In this regard, it is noteworthy that MKL1 and MKL2 are expressed in undifferentiated ES cells, whereas myocardin is expressed several days after the initiation of differentiation in vitro. Nevertheless, the demonstrated block in multiple genes encoding TGFβ/BMP family members in *Mkl2*$^{-/-}$ ES cells reveals a non-redundant function for MKL2 in ES cells in this context. Similarly, even though myocardin, MKL1 and MKL2 are co-expressed in vascular SMCs, only *Mkl2*$^{-/-}$ embryos demonstrate a block in TGFβ signaling in the embryonic vasculature, revealing a unique and non-redundant function of MKL2 in select arteries and vascular beds. However, it remains possible, indeed likely, that other TGF-β/BMP signaling molecules contributed to the vascular phenotype observed in *Mkl2*$^{-/-}$ mutant embryos. In support of this hypothesis, *Tgfb2*$^{-/-}$ embryos exhibit defects in pharyngeal arch development, but fail to phenocopy *Mkl2*$^{-/-}$ embryos (Gittenberger-de Groot et al., 2006; Sanford et al., 1997). By contrast, *Tgfb2/Tgfb3* compound mutant embryos recapitulate multiple aspects of the vascular changes observed in *Mkl2*$^{-/-}$ embryos (Dünker and Krieglstein, 2002).

Previous studies have shown that TGFβ2 and its cognate receptors, TGFBR2 and TGFBR1/ALK5, play a crucial role in embryonic angiogenesis and cardiovascular development (for a review, see Pardali et al., 2010). Both *Mkl2* and *Tgfb2* knockout mice exhibit aortic arch malformations involving the 4th pharyngeal arch artery (Gittenberger-de Groot et al., 2006; Sanford et al., 1997). However, *Mkl2*$^{-/-}$ embryos exhibit aneurysmal dilation of the aortic arch and carotid arteries, whereas *Tgfb2*$^{-/-}$embryos exhibit defects in vascular patterning attributable to the 4th pharyngeal arch artery. What explains these differences? As a transcriptional co-activator, MKL2 regulates and coordinates expression of multiple SRF-dependent genes involved in angiogenesis. Indeed, TGFβ2 and TGFβ3 are expressed in the great arteries during embryonic development (supplementary material Fig. S4A-L) and both isoforms were markedly repressed in *Mkl2*$^{-/-}$ ES cells (Fig. 3A; supplementary material Fig. S3). Moreover, expression of genes encoding TGFβ receptors and multiple Smads were downregulated in *Mkl2*$^{-/-}$ ES cells (Fig. 3; supplementary material Fig. S3). As such, the observed differences in phenotype between *Mkl2*$^{-/-}$ and *Tgfb2*$^{-/-}$ embryos most probably result from the differential expression of SRF/MKL2-regulated genes beyond TGFβ2. As discussed above, these include both genes encoding SMC contractile proteins, as well as related TGFβ/BMP signaling molecules.

The observation that *Mkl2*$^{-/-}$ mutant embryos develop aortic aneurysms accompanied by downregulation of TGFβ isoforms, TGFβ signaling and TGFβ-regulated genes encoding ECM strongly supports a model wherein loss of function of TGFβ signaling in the vasculature leads to aneurysm formation during embryonic angiogenesis. Consistent with this observation, conditional ablation of the *Tgfbr2* gene in vascular SMCs recapitulated many of the features observed in *Mkl2*$^{-/-}$ embryos, including aneurysmal dilation and dissection of the aorta during late embryonic development (Choudhary et al., 2009). However, these conclusions conflict with the observation that individuals with Marfan syndrome and Loeys-Dietz syndrome exhibit activation of TGFβ signaling and gain of TGFβ function in the arterial wall (Pearson et al., 2008). Interestingly, however, the NHLBI Go Exome Sequencing Project recently described a loss-of-function mutation in *TGFB2* that is associated with familial thoracic aortic aneurysms and acute aortic dissections associated with mild system features of Marfan syndrome (Boileau et al., 2012). These data highlight gaps in current understanding of the role that TGFβ signaling plays in the embryonic and adult vasculature, and suggests that TGFβ signals are differentially transduced during embryonic and postnatal development. In any case, further studies examining the role of MKL2 and/or MKL1 in maintenance and adaptation of the adult vasculature to hemodynamic stress promise to provide important new insights into the pathogenesis of heritable and acquired forms of vascular disease involving aneurysm formation and dissection.

Acknowledgements
We thank Jon Epstein, Mark Kahn and Ed Morrisey for their advice and helpful comments.

Funding
This work was supported in part by the National Institutes of Health (NIH) [R01-HL102968 and R01-HL094520 to M.S.P., T32-HL0783 to N.B.] and by the Commonwealth of Pennsylvania [to the University of Pennsylvania Cardiovascular Institute]. Deposited in PMC for release after 12 months.

Competing interests statement
The authors declare no competing financial interests.

Supplementary material
Supplementary material available online at
http://dev.biologists.org/lookup/suppl/doi:10.1242/dev.082222/-/DC1

References

Astrof, S. and Hynes, R. O. (2009). Fibronectins in vascular morphogenesis. *Angiogenesis* **12**, 165-175.
Astrof, S., Crowley, D. and Hynes, R. O. (2007). Multiple cardiovascular defects caused by the absence of alternatively spliced segments of fibronectin. *Dev. Biol.* **311**, 11-24.
Boileau, C., Guo, D. C., Hanna, N., Regalado, E. S., Detaint, D., Gong, L., Varret, M., Prakash, S. K., Li, A. H., d'Indy, H. et al.; National Heart, Lung, and Blood Institute (NHLBI) Go Exome Sequencing Project (2012). TGFB2 mutations cause familial thoracic aortic aneurysms and dissections associated with mild systemic features of Marfan syndrome. *Nat. Genet.* doi:10.1038/ng.2348.

Choudhary, B., Zhou, J., Li, P., Thomas, S., Kaartinen, V. and Sucov, H. M. (2009). Absence of TGFbeta signaling in embryonic vascular smooth muscle leads to reduced lysyl oxidase expression, impaired elastogenesis, and aneurysm. *Genesis* **47**, 115-121.

Du, K. L., Ip, H. S., Li, J., Chen, M., Dandre, F., Yu, W., Lu, M. M., Owens, G. K. and Parmacek, M. S. (2003). Myocardin is a critical serum response factor cofactor in the transcriptional program regulating smooth muscle cell differentiation. *Mol. Cell. Biol.* **23**, 2425-2437.

Du, K. L., Chen, M., Li, J., Lepore, J. J., Mericko, P. and Parmacek, M. S. (2004). Megakaryoblastic leukemia factor-1 transduces cytoskeletal signals and induces smooth muscle cell differentiation from undifferentiated embryonic stem cells. *J. Biol. Chem.* **279**, 17578-17586.

Dünker, N. and Krieglstein, K. (2002). Tgfbeta2 –/– Tgfbeta3 –/– double knockout mice display severe midline fusion defects and early embryonic lethality. *Anat. Embryol. (Berl.)* **206**, 73-83.

Gittenberger-de Groot, A. C., Azhar, M. and Molin, D. G. (2006). Transforming growth factor beta-SMAD2 signaling and aortic arch development. *Trends Cardiovasc. Med.* **16**, 1-6.

Guo, D. C., Pannu, H., Tran-Fadulu, V., Papke, C. L., Yu, R. K., Avidan, N., Bourgeois, S., Estrera, A. L., Safi, H. J., Sparks, E. et al. (2007). Mutations in smooth muscle α-actin (ACTA2) lead to thoracic aortic aneurysms and dissections. *Nat. Genet.* **39**, 1488-1493.

Hayward, I. P., Bridle, K. R., Campbell, G. R., Underwood, P. A. and Campbell, J. H. (1995). Effect of extracellular matrix proteins on vascular smooth muscle cell phenotype. *Cell Biol. Int.* **19**, 839-846.

Huang, J., Cheng, L., Li, J., Chen, M., Zhou, D., Lu, M. M., Proweller, A., Epstein, J. A. and Parmacek, M. S. (2008). Myocardin regulates expression of contractile genes in smooth muscle cells and is required for closure of the ductus arteriosus in mice. *J. Clin. Invest.* **118**, 515-525.

Lee, E. C., Yu, D., Martinez de Velasco, J., Tessarollo, L., Swing, D. A., Court, D. L., Jenkins, N. A. and Copeland, N. G. (2001). A highly efficient Escherichia coli-based chromosome engineering system adapted for recombinogenic targeting and subcloning of BAC DNA. *Genomics* **73**, 56-65.

Li, J., Zhu, X., Chen, M., Cheng, L., Zhou, D., Lu, M. M., Du, K., Epstein, J. A. and Parmacek, M. S. (2005). Myocardin-related transcription factor B is required in cardiac neural crest for smooth muscle differentiation and cardiovascular development. *Proc. Natl. Acad. Sci. USA* **102**, 8916-8921.

Massagué, J. (1990). The transforming growth factor-beta family. *Annu. Rev. Cell Biol.* **6**, 597-641.

Molin, D. G., Bartram, U., Van der Heiden, K., Van Iperen, L., Speer, C. P., Hierck, B. P., Poelmann, R. E. and Gittenberger-de-Groot, A. C. (2003). Expression patterns of Tgfbeta1-3 associate with myocardialisation of the outflow tract and the development of the epicardium and the fibrous heart skeleton. *Dev. Dyn.* **227**, 431-444.

Molin, D. G., Poelmann, R. E., DeRuiter, M. C., Azhar, M., Doetschman, T. and Gittenberger-de Groot, A. C. (2004). Transforming growth factor β-SMAD2 signaling regulates aortic arch innervation and development. *Circ. Res.* **95**, 1109-1117.

Morisaki, H., Akutsu, K., Ogino, H., Kondo, N., Yamanaka, I., Tsutsumi, Y., Yoshimuta, T., Okajima, T., Matsuda, H., Minatoya, K. et al. (2009). Mutation of ACTA2 gene as an important cause of familial and nonfamilial nonsyndromatic thoracic aortic aneurysm and/or dissection (TAAD). *Hum. Mutat.* **30**, 1406-1411.

Morrisey, E. E., Tang, Z., Sigrist, K., Lu, M. M., Jiang, F., Ip, H. S. and Parmacek, M. S. (1998). GATA6 regulates HNF4 and is required for differentiation of visceral endoderm in the mouse embryo. *Genes Dev.* **12**, 3579-3590.

Mouilleron, S., Langer, C. A., Guettler, S., McDonald, N. Q. and Treisman, R. (2011). Structure of a pentavalent G-actin*MRTF-A complex reveals how G-actin controls nucleocytoplasmic shuttling of a transcriptional coactivator. *Sci. Signal.* **4**, ra40.

Oh, J., Richardson, J. A. and Olson, E. N. (2005). Requirement of myocardin-related transcription factor-B for remodeling of branchial arch arteries and smooth muscle differentiation. *Proc. Natl. Acad. Sci. USA* **102**, 15122-15127.

Owens, G. K. (1998). Molecular control of vascular smooth muscle cell differentiation. *Acta Physiol. Scand.* **164**, 623-635.

Owens, G. K., Kumar, M. S. and Wamhoff, B. R. (2004). Molecular regulation of vascular smooth muscle cell differentiation in development and disease. *Physiol. Rev.* **84**, 767-801.

Pardali, E., Goumans, M.-J. and ten Dijke, P. (2010). Signaling by members of the TGF-β family in vascular morphogenesis and disease. *Trends Cell Biol.* **20**, 556-567.

Parmacek, M. S. (2007). Myocardin-related transcription factors: critical coactivators regulating cardiovascular development and adaptation. *Circ. Res.* **100**, 633-644.

Pearson, G. D., Devereux, R., Loeys, B., Maslen, C., Milewicz, D., Pyeritz, R., Ramirez, F., Rifkin, D., Sakai, L., Svensson, L. et al.; National Heart, Lung, and Blood Institute and National Marfan Foundation Working Group (2008). Report of the National Heart, Lung, and Blood Institute and National Marfan Foundation Working Group on research in Marfan syndrome and related disorders. *Circulation* **118**, 785-791.

Raines, E. W. (2000). The extracellular matrix can regulate vascular cell migration, proliferation, and survival: relationships to vascular disease. *Int. J. Exp. Pathol.* **81**, 173-182.

Regalado, E., Medrek, S., Tran-Fadulu, V., Guo, D. C., Pannu, H., Golabbakhsh, H., Smart, S., Chen, J. H., Shete, S., Kim, D. H. et al. (2011). Autosomal dominant inheritance of a predisposition to thoracic aortic aneurysms and dissections and intracranial saccular aneurysms. *Am. J. Med. Genet. A.* **155**, 2125-2130.

Sanford, L. P., Ormsby, I., Gittenberger-de Groot, A. C., Sariola, H., Friedman, R., Boivin, G. P., Cardell, E. L. and Doetschman, T. (1997). TGFbeta2 knockout mice have multiple developmental defects that are non-overlapping with other TGFbeta knockout phenotypes. *Development* **124**, 2659-2670.

Sotiropoulos, A., Gineitis, D., Copeland, J. and Treisman, R. (1999). Signal-regulated activation of serum response factor is mediated by changes in actin dynamics. *Cell* **98**, 159-169.

Subramanian, A., Tamayo, P., Mootha, V. K., Mukherjee, S., Ebert, B. L., Gillette, M. A., Paulovich, A., Pomeroy, S. L., Golub, T. R., Lander, E. S. et al. (2005). Gene set enrichment analysis: a knowledge-based approach for interpreting genome-wide expression profiles. *Proc. Natl. Acad. Sci. USA* **102**, 15545-15550.

Thyberg, J. and Hultgårdh-Nilsson, A. (1994). Fibronectin and the basement membrane components laminin and collagen type IV influence the phenotypic properties of subcultured rat aortic smooth muscle cells differently. *Cell Tissue Res.* **276**, 263-271.

Wang, D. Z., Li, S., Hockemeyer, D., Sutherland, L., Wang, Z., Schratt, G., Richardson, J. A., Nordheim, A. and Olson, E. N. (2002). Potentiation of serum response factor activity by a family of myocardin-related transcription factors. *Proc. Natl. Acad. Sci. USA* **99**, 14855-14860.

Wei, K., Che, N. and Chen, F. (2007). Myocardin-related transcription factor B is required for normal mouse vascular development and smooth muscle gene expression. *Dev. Dyn.* **236**, 416-425.

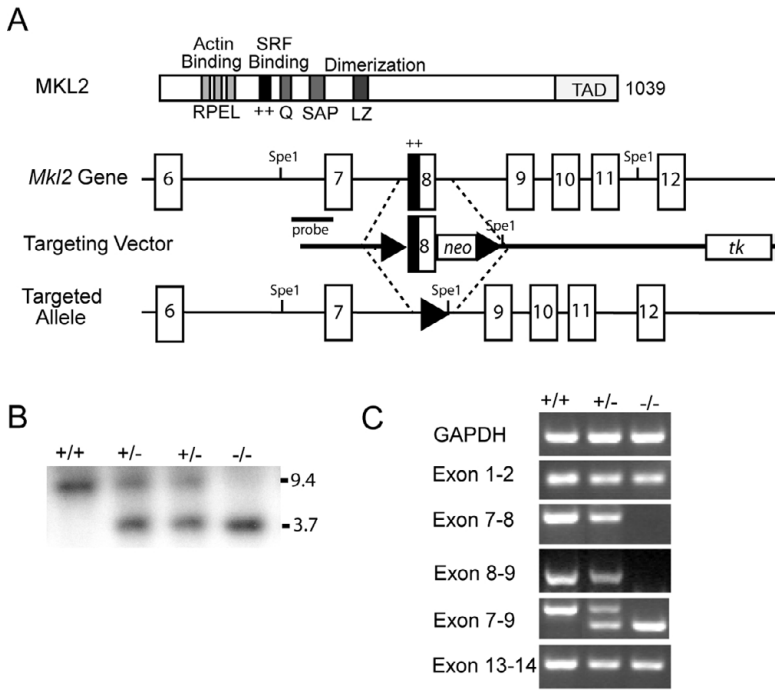

Fig. S1. Generation and characterization of *Mkl 2*$^{-/-}$ null embryos. (**A**) Schematic representation of the MKL2 protein and the gene targeting strategy used in this manuscript. The locations of the RPEL, Basic, Glutamine-rich (Q), SAP and transcriptional activation (TD) domains and leucine zipper (LZ) are shown. A schematic representation of exons 6-12 (rectangles) of the mouse *Mkl2* gene, including the location restriction enzyme sites used to genotype ES cells and mice. The position of the DNA probe used for Southern blot analysis is indicated below (black rectangle). The targeted allele contains the PGK-neomycin resistance (neo) cassette and loxP sites (triangles) flanking exon 8. (**B**) Southern blot analysis of mouse genomic DNA demonstrating the 9.4 kb wild-type allele (+) and the 3.7 kb null allele generated after Cre-mediated recombination. (**C**) PCR genotype analysis showing the expected bands corresponding to the wild-type allele (+) and conditionally targeted allele (–) following Cre-mediated recombination. PCR primers complementing the specific exons indicated are shown on the right of the ethidium bromide-stained agarose gel.

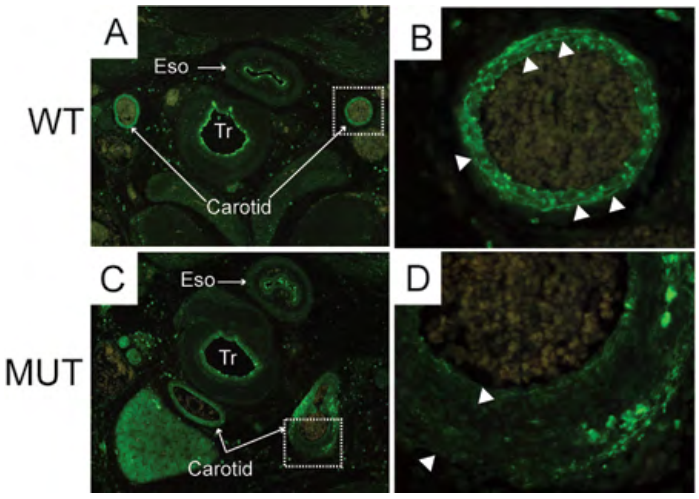

Fig. S2. Disruption of elastin organization in the carotid artery of E13.5 *Mkl2*$^{-/-}$ mutant embryos. Histological sections were prepared from E13.5 wild-type (WT) and *Mkl2*$^{-/-}$ (MUT) embryos were immunostained with anti-tropoelastin antibody (green). (**A**,**C**) Histological transverse sections cut at the level of the common carotid arteries in wild-type control (A) and *Mkl2*$^{-/-}$ mutant (MUT) embryo. The location of the trachea (Tr) and esophagus (Eso) are shown. The white rectangles indicate the sections shown in B and D. Original magnification was ×40. (**B**,**D**) High-power magnification reveals the structure of the tunica media in the left common carotid artery in a wild-type (B) and mutant (D) embryo. In the wild-type carotid, thin elastin fibers (arrows, green stain) are visualized between layers of spindle shaped vascular SMCs. By contrast, medial organization of the mutant artery is disrupted with attenuated or absence of tropoelastic staining in segments of the artery (arrows) and irregular deposition of elastin in other other segments. Original magnification was ×400.

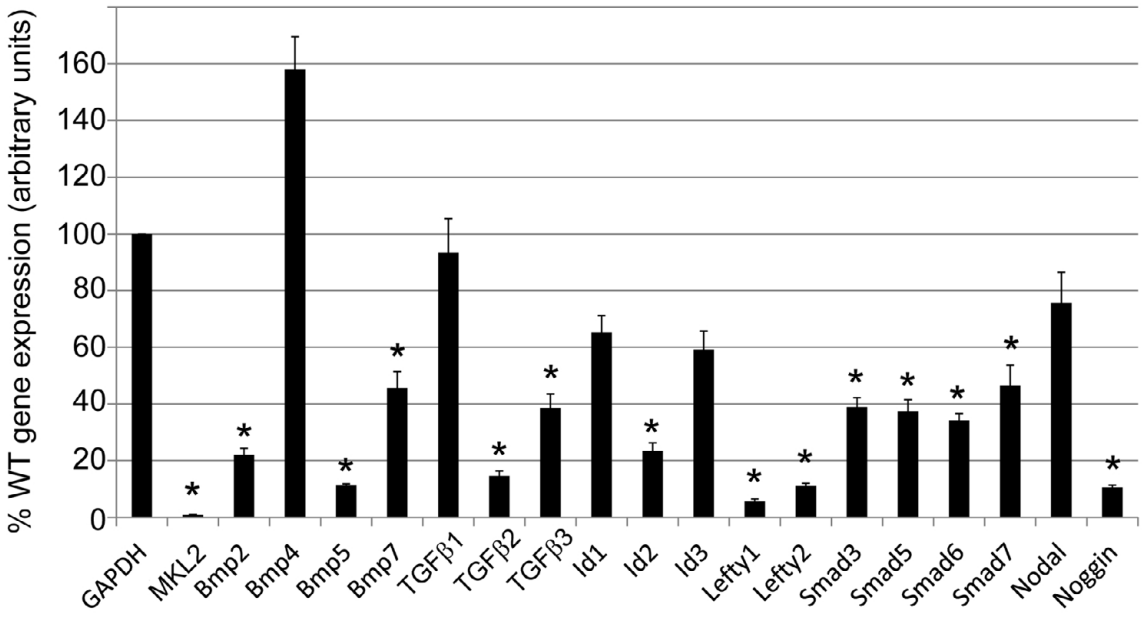

Fig. S3. Multiple TGF-β/BMP genes are downregulated in *Mkl2*$^{-/-}$ ES cells. To validate the microarray studies, qRT-PCR analyses were performed with mRNA harvested from wild-type and *Mkl2*$^{-/-}$ ES cells. The experiment was performed three times with three biological replicates used in each experiment. Data are expressed as the percentage of wild-type gene expression (arbitrary units) observed in *Mkl2*$^{-/-}$ ES cells±s.e.m. (**P*<0.01 versus wild-type gene expression).

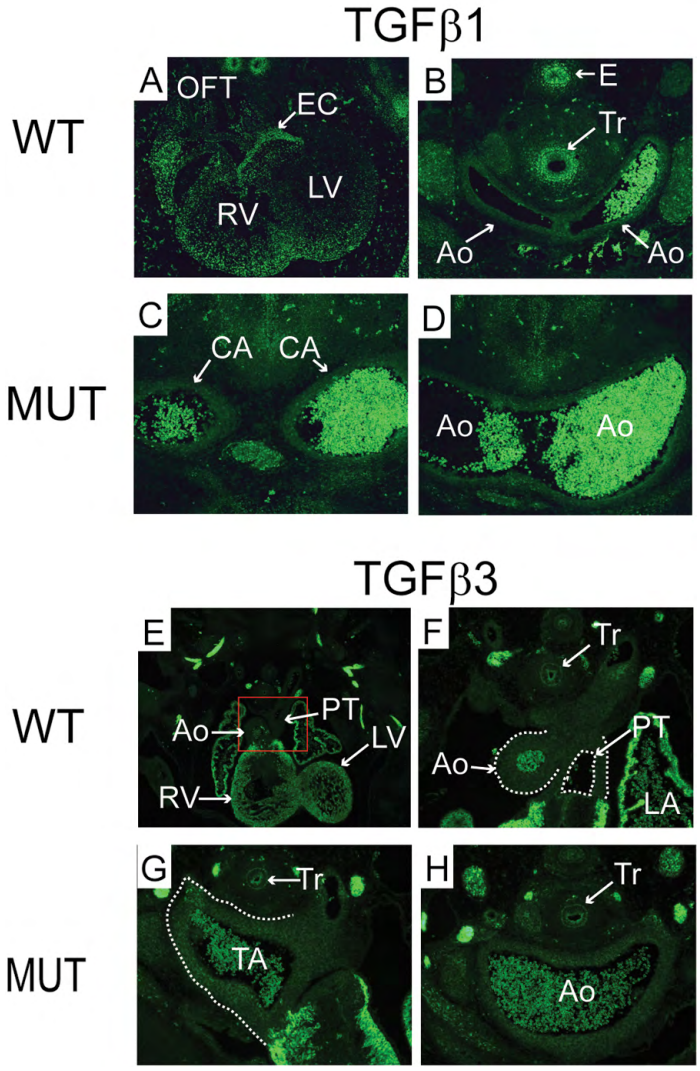

Fig. S4. Expression of TGFβ1 and TGFβ3 in the cardiac outflow tract and great arteries of E14.5 control and *Mkl2*$^{-/-}$ embryos. Histological sections cut at the level of the cardiac outflow tract of wild-type (WT) control and *Mkl2*$^{-/-}$ mutant embryos were immunostained with antibodies that recognize TGFβ1 (A-D) or TGFβ3 (E-H). (**A-D**) Abundant TGFβ1 (green stain) is observed throughout the embryonic RV and LV myocardium and endocardial cushions (EC) (A). By contrast, TGFβ1 (green stain) was expressed background levels (IgG) in the aortic arch (Ao) and carotid arteries (CA). The location of the trachea (Tr) and esophagus (E) are shown. Original magnifications were ×20 in A; ×100 in B-D. (**E**,**F**) Abundant TGFβ3 (green stain) is observed throughout the LV and RV myocardium of the control embryo. The red rectangle in E demarcates the location of F. By contrast, very low levels of TGFβ3 are observed in the ascending aorta (Ao) and pulmonary trunk (PT), whereas abundant TGFβ3 is observed in the LA. (**G**,**H**) In addition, low levels of TGFβ3 are observed in the wall of the truncus arteriosus (TA) and arch of the aorta (Ao) of *Mkl2*$^{-/-}$ mutant embryos. No appreciable difference in TGFβ3 expression was observed in the great arteries of wild-type and MUT embryos. Original magnifications were ×20 in E and ×100 in F-H.

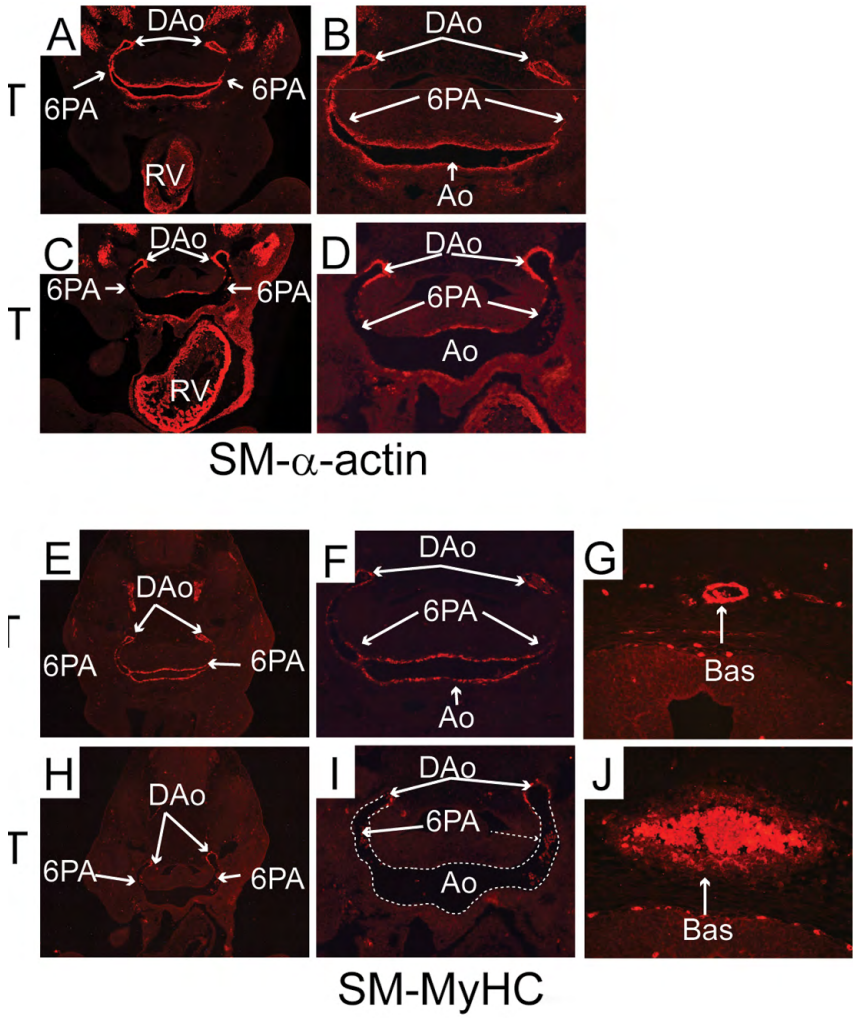

Fig. S5. Expression of SMC contractile proteins is downregulated in arteries of *Mkl2*$^{-/-}$ mutant embryos. (**A-D**) Histological sections prepared from E9.5 wild-type control (A,B) and *Mkl2*$^{-/-}$ mutant (MUT) embryos were immunostained with SM-α-actin (SMA) antibody. (A,B) Abundant SMA (red) is observed throughout the embryonic RV, pharyngeal arch arteries (6PA) and dorsal aorta (DAo) in wild-type embryos. (C,D) By contrast, expression of SMA is markedly attenuated in the pharyngeal arch arteries (6PA) and aorta (Ao) of *Mkl2*$^{-/-}$ mutant embryos. Of note, SMA expression is preserved in the dorsal aorta (DAo) and embryonic RV. Original magnifications were ×50 in A,C; ×100 in B,D. (**E-J**) Histological sections prepared from E9.5 wild-type control (E-G) and *Mkl2*$^{-/-}$ MUT (H-J) embryos were immunostained with SM-myosin heavy chain (SM-MyHC) antibody. (E,F) Abundant SM-MyC (red) is observed throughout the pharyngeal arch arteries (6PA) and dorsal aorta (DAo) in wild-type embryos. (H,I) By contrast, expression of SM-MyHC is markedly attenuated in the pharyngeal arch arteries (6PA) and aorta (Ao) of *Mkl2*$^{-/-}$ mutant embryos. Once again, SM-MyHC expression is preserved in the dorsal aorta (DAo). (G,J). Histological sections showing the basilar artery (Bas) demonstrating that expression of SM-MyHC is markedly attenuated in the mutant basilar artery (J) compared with the basilar artery in the wild-type embryo (G). Original magnifications were ×50 in E,H, ×100 in F,I and ×200 in G,J.

Table S1. PCR primers used in these studies

***Mkl2* genotyping primers**

P1	F,5'-ATACAACCCGCTTTTTAATAGG-3'
P2	F,5'-ATCTGTACAGCTTGAAACCTGGCC-3'
P3	R, 5'-TTCCCATTTCCACACGCTGATGTT-3'

qRT-PCR primers

GAPDH	F, 5'-AGTCCATGCCATCACTGCCACCCA-3' R, 5'-TCCACCACCCTGTTGCTGTAGCCG-3'
SRF	F, 5'-CCCGCTCAGACCCCACCACAGA-3' R, 5'-CAGGTAGTTGGTGATGGGGAAGGA-3'
MKL1	F, 5'-ACACTCATCAAGCAAAGCCAACCC-3', R,5'-GATCTTGGCATAGGAGGAGTCCAT-3'
MKL2	F, 5'-AACCCCTCTAACTGCAGAC-3' R,5'-GCTACGGTGTTTGTCGTTTG-3'
TGFβ1	F, 5'-ACCCTGCCCCTATATTTGGA-3', R,5'- TGGTTGTAGAGGGCAAGGAC-3'
TGFβ2	F,5'-GAACCCAAAGGGTACAATGC-3', R,5'-TGGTGTTGTACAGGCTGAGG-3'
TGFβ3	F,5'-TATGCCAACTTCTGCTCAGG-3' R,5'-CTCTGGGTTCAG GGTGTTGT-3'
SMA	F,5-'TACCATGTACCCTGGCATTGCTGA-3' R,5-'AGAAGGCCCTCTGACTTTAGAAGC-3'
SMMyHC	F, 5'-CTCTGTGCTGCACAACCTGA-3' R, 5'-TCGGCAATGGCATAGATGTG-3'
Fn	F, 5'-AGACCTGGGAAAAGCCCTACCAA-3' R, 5'-ACTGAAGCAGGTTTCCTCGGTTGT-3'
Col4a1	F, 5'-TGGATCGGCTATTCCTTCG-3' R,5'-GGCGCTTCTAAACTCTTCC-3'
Fbn1	F,5'-CTGTCCACCAGGATACTTCC-3' R,5'-CAGTGAGTTGTCGTCCATC-3'
Itgα5	F,5'-GCACCACCATTCAATTTGAC-3' R,5'-CACTGCAAGGACTTGTACTC-3'
Itgβ5	F,5'-GAATGCCTGTTGATCCACC-3' R,5'-GGATGAGGTTTGCCTTCAG-3'
Itgβ8	F,5'-CTGCAAATGTGGTCTCCTGTGC-3' R,5'-CGTTCACTTCCTGATCCACCTG-3'
Talin	F,GCTCGGGCGTTAGCAGTC-3' R,ATGGAATCTGAGACAGTCCGAGA-3'
Vinculin	F,5'-CCAAGGTCAGAGAAGCCTTCC-3' R,5'-CGTAGCTGTTCAAGGTCTGGTG-3'
Id1	F,5'-GGAGATCCTGCAGCATGTAATC-3' R,5'-ATCGTCGGCTGGAACACATG-3'
Id2	F,5'-TGGACTCGCATCCCACTATC-3' R,5'-CATTCGACATAAGCTCAGAAGG-3'

Id3	5’-GCGTGTCATAGACTACATCCTC-3’ R,5’-CCTCTTGTCCTTGGAGATCAC-3’
Bmp2	F,5’-GAATCAGAACACAAGTCA GT-3’ R,5’-GTTTGTGTTTGGCTTGACGC-3’
Bmp4	F,5’-TGTGAGGAGTTTCCATCACG-3’ R,5’-CAGCGAAGGACTGCAGGGCT-3’
Bmp5	F, 5’-GGATGGCCGCAGCATCAATGTAAA-3’ R, 5’-GAAGGCCACCATGAATGGCTGTTT-3’
Bmp7	F, 5’-ACCGCAGCCGAATTCAGGATCTAT-3’ R, 5’-TATCAAACACCAACCAGCCCTCCT-3’
Smad3	F,5’- CCAGGCTGACATGGGCAAATGAAA-3’ R, 5’-TGTCACAGTTTGCTGTGGCAATCC-3’
Smad5	F, 5’-AGCAAGAGTGTGTCAGCTCCATGA-3’ R,5’- TCCTGAAGGCTGCCAAGTAAAGGA-3’
Smad6	F, 5’-ACAAGCCACTGGATCTGTCCGATT-3’ R, 5’-AGAATTCACCCGGAGCAGTGATGA-3’
Smad7	F, 5’-TTCGGACAACAAGAGTCAGCTGGT-3’ R, 5’-AGCCTTGATGGAGAAACCAGGGAA-3’
Smad9	F,5’- TGACGGCAGGTACATTCAACCAGA-3’ R,5’- TTAAGAGCCTTGGCTTTGCTTGCC-3’
Lefty1	F,5’-ATGATTGTCAGCGTGAAGGAGGGA-3’ R,5’- TTGCATGAAAGGCACATCCTTGGG-3’
Lefty2	F,5’-TCCTGACGTATGAATGTGTGGGCA-3’ R,5’- ACTGACAATCATGGGCAAGGAGGT-3’
Nodal	F,5’- ACATGATTGTGGAGGAGTGTGGGT-3’, R,5’- TCTTTAGCTCCAGCAGGCAGAACT-3’
Noggin	F,5’-TGAGCAAGAAGCTGAGGAGGAAGT-3’ R,5’-AGGTGCACAGACTTGGATGGCTTA-3’
Pitx2	F,5’-ATG GAG ACC AAT TGT CGC AAA C-3’, R,5’-GCT TCC GTA AGG TTG GTC CAC A-3’

ChIP assay primers

Control	F,5’-ATGCTAAGTAATGGGACATTGCT-3’ R,5’-AAGTCAGCTCTGCTTCCAGG-3’
CArG1	F,5’-CTGGGGCTGACCTTGAAGGAAGAA-3’ R,5’-TTCTTCTACTCCACTGGCCCTGAG-3’
CArG2	F,5’-ATGGGGACCAAACCCAAAGGAT-3’, R,5’-ACTTCTCTACGCAAAGGGCACTG-3’
CArG3	F,5’-AAACAGTTGGGTCCCGTCCA-3’ R,5’-GAACACTATTCTGGGAGCCA,-3’
CArG4	F,5’-CTATCCCTTTCACTCCCGAGCTGTC-3’ R,5’-ACACACACACACACACACACATGAC-3’
CArG5	F,5’-GTGGTTGATTTTCATGTTGTGG-3’ R,5’-CAGAGAGTCTGCCTTTTTAGG-3’

Table S2. Primary and secondary antibodies used in these studies

Primary antibodies	**Catalog code**	**Vendor**
polyclonal anti-fibronectin	NB100-92247	Novus Biologicals
monoclonal anti-fibronectin	sc-8422	Santa Cruz Biotechnology
polyclonal anti-GAPDH	G9545	Sigma
polyclonal anti-β-tubulin	ab6046	Abcam
polyclonal anti-tropoelastin	ab21601	Abcam
monoclonal anti-phospho Smad3	CG1561	Cell Applications
monoclonal anti-TGFβ2	MAB612	R&D systems
monoclonal anti-smooth muscle-actin (1A4)	A5228	Sigma-Aldrich
polyclonal anti-phospho-paxillin (Tyr118)	2541	Cell Signaling Technology
polyclonal anti-collagen IV	AB756P	Millipore
polyclonal Anti-SRF (G20)	sc335	Santa Cruz
Rabbit IgG	2729	Cell Signaling Technology
Secondary antibodies		
Alexa Fluor® 488 Goat Anti-Mouse IgG	A-11001	Invitrogen
Alexa Fluor® 488 Rabbit Anti-Mouse IgG	A-11059	Invitrogen
Alexa Fluor® 568 Goat Anti-Rabbit IgG	A11011	Invitrogen
Alexa Fluor® 568 Goat Anti-Mouse IgG	A-11004	Invitrogen
Alexa Fluor® 594 Donkey Anti-Goat IgG (H+L)	705-585-003	Jackson ImmunoResearch
Donkey anti-mouse IgG HRP	715-035-150	Jackson ImmunoResearch

Table S3. Genes induced or repressed by twofold or more in response to *Mkl2* deletion
Owing to the small number of replicates, no statistical analysis is provided and data are regarded as exploratory

Induced genes			
Transcript cluster	**Gene symbol**	**mRNA Accession Number**	**Fold change (*Mkl2*$^{-/-}$ versus control)**
10369615	Srgn	NM_011157	30.57
10480155	Cubn	NM_001081084	7.32
10458262	Slc23a1	NM_011397	3.14
10561153	Cyp2b23	NM_001081148	3.02
10499412	Rab25	NM_016899	2.91
10446473	Lama1	NM_008480	2.74
10484276	Neurod1	NM_010894	2.34
10351368	Gpa33	NM_021610	2.20
10436978	Cbr3	NM_173047	2.16
10474575	Slc12a6	BC062099	2.02
10570516	Kbtbd11	BC080858	2.00
Repressed genes			
Transcript cluster	**Gene symbol**	**mRNA Accession Number**	**Fold change (*Mkl2*$^{-/-}$ versus control)**
10606837	Nxf3	NM_001024141	0.50
10369388	Unc5b	NM_029770	0.50
10397346	Fos	NM_010234	0.50
10454701	Wnt8a	NM_009290	0.49
10604961	Gabra3	NM_008067	0.49
10569344	Igf2	NM_001122737	0.49
10602925	Phka2	NM_172783	0.49
10359161	Soat1	NM_009230	0.49
10519951	Pion	NM_175437	0.49
10427402	Ghr	NM_010284	0.49
10408937	Atxn1	NM_009124	0.49
10377938	Eno3	NM_007933	0.48
10444258	Psmb8	NM_010724	0.48
10352320	Tmem63a	NM_144794	0.48
10503835	Rragd	NM_027491	0.48
10505132	Akap2	NM_001035533	0.48
10583203	Phxr4	BC107288	0.48
10602805	Mtap7d2	NM_001081124	0.48
10560481	Fosb	NM_008036	0.48
10347277	Igfbp2	NM_008342	0.48

10484307	Frzb	NM_011356	0.47
10513256	Lpar1	NM_010336	0.47
10406270	Glrx	NM_053108	0.47
10461629	Ms4a4d	NM_025658	0.47
10415411	Nynrin	BC057379	0.47
10545780	Exoc6b	BC145693	0.47
10599120	Dock11	NM_001009947	0.47
10571601	Pdlim3	NM_016798	0.47
10385036	Fgf18	NM_008005	0.47
10361771	Plagl1	NM_009538	0.47
10485982	Actc1	NM_009608	0.47
10442194	Zfp677	NM_172486	0.46
10604633	Cxx1b	NM_001018063	0.46
10406229	Pcsk1	NM_013628	0.46
10497817	Anxa5	NM_009673	0.46
10366546	Cpm	NM_027468	0.46
10468070	Fgf8	NM_010205	0.46
10606609	Tspan6	NM_019656	0.46
10469936	Nrarp	NM_025980	0.46
10496569	Gbp6	NM_001083312	0.46
10533050	Hspb8	NM_030704	0.46
10499132	Mab21l2	NM_011839	0.46
10543145	Thsd7a	AK173072	0.46
10406205	Erap1	NM_030711	0.45
10541524	Nanog	NM_028016	0.45
10431915	Slc38a4	NM_027052	0.45
10601980	Mum1l1	NM_175541	0.45
10359870	Pbx1	NM_183355	0.44
10505028	Slc44a1	AK141895	0.44
10496580	Gbp3	NM_018734	0.44
10576495	Trim67	BC094596	0.44
10604576	Gpc3	NM_016697	0.43
10429564	Ly6a	NM_010738	0.43
10544089	Zc3hav1	NM_028864	0.42
10449807	Abhd9	NM_001033163	0.42
10496555	Gbp1	NM_010259	0.42
10362097	H60b	AB284505	0.42
10474229	Cd59a	NM_001111060	0.42
10570957	Sfrp1	NM_013834	0.42
10534667	Serpine1	NM_008871	0.42
10464905	Npas4	NM_153553	0.41

10472688	Sp5	NM_022435	0.41
10497149	Gpr177	NM_026582	0.41
10607562	Cnksr2	NM_177751	0.41
10357137	Gli2	NM_001081125	0.40
10603208	Mid1	NM_010797	0.40
10538590	Herc5	ENSMUST00000031817	0.40
10509163	Id3	NM_008321	0.40
10496592	Gbp2	NM_010260	0.39
10603289	Clcn5	NM_016691	0.39
10352302	Lefty2	NM_177099	0.39
10438603	Igf2bp2	NM_183029	0.39
10521471	Ppp2r2c	NM_172994	0.39
10549964	Zscan4c	NM_001013765	0.38
10371379	Nuak1	NM_001004363	0.38
10544596	Tmem176b	NM_023056	0.38
10531420	Cxcl11	NM_019494	0.38
10578829	Palld	NM_001081390	0.38
10549972	Zscan4c	NM_001013765	0.38
10607587	Pdha1	NM_008810	0.37
10587639	Nt5e	NM_011851	0.37
10469167	Sfmbt2	NM_177386	0.37
10429568	Ly6c1	NM_010741	0.37
10498018	Pcdh18	NM_130448	0.36
10344966	Ly96	NM_016923	0.36
10592251	Pknox2	NM_001029838	0.36
10477920	Myl9	NM_172118	0.36
10607524	Sms	NM_009214	0.35
10361358	Rgs17	NM_019958	0.35
10583809	Cnn1	NM_009922	0.34
10604844	Sms	AF031486	0.34
10559978	Zscan4c	NM_001013765	0.34
10428619	Enpp2	NM_015744	0.34
10384223	Igfbp3	NM_008343	0.33
10407435	Akr1c18	NM_134066	0.33
10604551	Usp26	NM_031388	0.33
10445293	Pla2g7	NM_013737	0.33
10477250	Hck	NM_010407	0.32
10397984	Ppp4r4	NM_028980	0.32
10376950	Pmp22	NM_008885	0.31
10459335	Fam38b	BC147606	0.30
10360920	Tgfb2	NM_009367	0.30

10344952	Rdh10	NM_133832	0.29
10607619	Cdkl5	NM_001024624	0.29
10374777	Efemp1	NM_146015	0.28
10593123	Tagln	NM_011526	0.26
10404429	Serpinb9	NM_009256	0.26
10599348	Gria3	NM_016886	0.26
10602772	Rps6ka3	NM_148945	0.26
10467124	Acta2	NM_007392	0.26
10387855	Alox15	NM_009660	0.25
10493850	Sprr2a	NM_011468	0.23
10602977	Scml2	NM_133194	0.16
10569335	H19	NR_001592	0.15
10608138	Ddx3y	NM_012008	0.09
10608107	Uty	NM_009484	0.08
10441669	T	NM_009309	0.07
10477986	Nnat	NM_010923	0.05

Table S4. KEGG pathways repressed in response to *Mkl2* deletion by Gene Set Enrichment Analysis

KEGG pathways (From MsigDB)	Number of genes	Normalized Enrichment Score (NES)	Nominal *P* value	FDR q-val
HSA04350_TGF_BETA_SIGNALING_PATHWAY	84	-2.067	0.0000	0.0000
HSA04360_AXON_GUIDANCE	125	-1.982	0.0000	0.0021
HSA04340_HEDGEHOG_SIGNALING_PATHWAY	53	-1.942	0.0000	0.0066
HSA05217_BASAL_CELL_CARCINOMA	53	-1.900	0.0000	0.0109
HSA04510_FOCAL_ADHESION	182	-1.774	0.0000	0.0656
HSA04010_MAPK_SIGNALING_PATHWAY	231	-1.745	0.0000	0.0785
HSA04310_WNT_SIGNALING_PATHWAY	133	-1.741	0.0000	0.0696
HSA01030_GLYCAN_STRUCTURES_BIOSYNTHESIS_1	102	-1.722	0.0000	0.0754
HSA00510_N_GLYCAN_BIOSYNTHESIS	36	-1.713	0.0102	0.0725
HSA05212_PANCREATIC_CANCER	70	-1.712	0.0029	0.0661
HSA04110_CELL_CYCLE	102	-1.712	0.0014	0.0601
HSA05210_COLORECTAL_CANCER	78	-1.689	0.0014	0.0698
HSA00640_PROPANOATE_METABOLISM	30	-1.677	0.0107	0.0731
HSA04320_DORSO_VENTRAL_AXIS_FORMATION	26	-1.677	0.0101	0.0679
HSA04662_B_CELL_RECEPTOR_SIGNALING_PATHWAY	60	-1.662	0.0030	0.0741
HSA05130_PATHOGENIC_ESCHERICHIA_COLI_INFECTION_EHEC	41	-1.642	0.0114	0.0845
HSA04810_REGULATION_OF_ACTIN_CYTOSKELETON	186	-1.619	0.0026	0.0964
HSA04520_ADHERENS_JUNCTION	70	-1.618	0.0073	0.0921
HSA00760_NICOTINATE_AND_NICOTINAMIDE_METABOLISM	21	-1.612	0.0269	0.0910
HSA04916_MELANOGENESIS	89	-1.596	0.0088	0.0999
HSA05131_PATHOGENIC_ESCHERICHIA_COLI_INFECTION_EPEC	41	-1.589	0.0144	0.1018
HSA00410_BETA_ALANINE_METABOLISM	24	-1.589	0.0339	0.0975
HSA00563_GLYCOSYLPHOSPHATIDYLINOSITOL_ANCHOR_BIOSYNTHESIS	19	-1.586	0.0204	0.0963
HSA00100_BIOSYNTHESIS_OF_STEROIDS	22	-1.558	0.0383	0.1162
HSA04530_TIGHT_JUNCTION	114	-1.555	0.0055	0.1147
HSA00561_GLYCEROLIPID_METABOLISM	46	-1.533	0.0411	0.1316
HSA05220_CHRONIC_MYELOID_LEUKEMIA	71	-1.532	0.0177	0.1281
HSA00512_O_GLYCAN_BIOSYNTHESIS	28	-1.521	0.0369	0.1339
HSA04620_TOLL_LIKE_RECEPTOR_SIGNALING_PATHWAY	88	-1.511	0.0226	0.1399
HSA04060_CYTOKINE_CYTOKINE_RECEPTOR_INTERACTION	208	-1.510	0.0063	0.1359
HSA00280_VALINE_LEUCINE_AND_ISOLEUCINE_DEGRADATION	40	-1.505	0.0305	0.1361
HSA01031_GLYCAN_STRUCTURES_BIOSYNTHESIS_2	51	-1.501	0.0250	0.1358
HSA05221_ACUTE_MYELOID_LEUKEMIA	49	-1.495	0.0363	0.1383
HSA04150_MTOR_SIGNALING_PATHWAY	42	-1.493	0.0422	0.1361
HSA05010_ALZHEIMERS_DISEASE	27	-1.462	0.0677	0.1653
HSA05211_RENAL_CELL_CARCINOMA	67	-1.459	0.0427	0.1631

HSA00380_TRYPTOPHAN_METABOLISM	50	-1.456	0.0541	0.1626
HSA00530_AMINOSUGARS_METABOLISM	26	-1.447	0.0689	0.1687
HSA04115_P53_SIGNALING_PATHWAY	57	-1.439	0.0365	0.1754
HSA00252_ALANINE_AND_ASPARTATE_METABOLISM	29	-1.433	0.0733	0.1770
HSA04660_T_CELL_RECEPTOR_SIGNALING_PATHWAY	89	-1.425	0.0418	0.1832
HSA00230_PURINE_METABOLISM	137	-1.409	0.0332	0.1976
HSA00120_BILE_ACID_BIOSYNTHESIS	31	-1.381	0.0983	0.2312
HSA00251_GLUTAMATE_METABOLISM	30	-1.378	0.0992	0.2301
HSA00650_BUTANOATE_METABOLISM	42	-1.378	0.0970	0.2251
HSA04120_UBIQUITIN_MEDIATED_PROTEOLYSIS	34	-1.376	0.0902	0.2239
HSA04930_TYPE_II_DIABETES_MELLITUS	41	-1.375	0.0927	0.2197
HSA00600_SPHINGOLIPID_METABOLISM	33	-1.374	0.1128	0.2168
HSA00020_CITRATE_CYCLE	25	-1.363	0.1036	0.2261
HSA03320_PPAR_SIGNALING_PATHWAY	57	-1.356	0.0922	0.2324
HSA04330_NOTCH_SIGNALING_PATHWAY	39	-1.346	0.1049	0.2411
HSA04130_SNARE_INTERACTIONS_IN_VESICULAR_TRANSPORT	30	-1.345	0.1197	0.2373
HSA04920_ADIPOCYTOKINE_SIGNALING_PATHWAY	68	-1.342	0.0708	0.2370
HSA00340_HISTIDINE_METABOLISM	36	-1.336	0.1130	0.2405
HSA04630_JAK_STAT_SIGNALING_PATHWAY	132	-1.326	0.0523	0.2493